Review

Mariano A. Kappes* and Teresa Perez

Hydrogen blending in existing natural gas transmission pipelines: a review of hydrogen embrittlement, governing codes, and life prediction methods

https://doi.org/10.1515/corrrev-2022-0083
Received September 12, 2022; accepted February 14, 2023; published online March 17, 2023

Abstract: Existing natural gas pipelines provide an economic alternative for the transport of hydrogen (H_2) in an envisioned hydrogen economy. Hydrogen can dissolve in the steel and cause hydrogen embrittlement (HE), compromising pipeline structural integrity. HE causes subcritical cracking, decreases ductility and fracture toughness, and increases the fatigue crack growth rate (FCGR). This work analyzes the testing standards in gaseous hydrogen used to quantify those effects. Design code ASME B31.12 applicable to hydrogen pipelines has more stringent requirements than ASME B31.8 code commonly used for constructing natural gas pipelines. Differences in materials requirements specified by those codes are summarized. ASME B31.12 pipeline code applies for H_2 at a concentration greater than 10% molar. However, recent testing programs acknowledge that H_2 degrades steel mechanical properties regardless of its percentage in the blend. This paper discusses how the hydrogen degraded mechanical properties affect pipeline integrity. Decreased mechanical properties cause a drop in the failure pressure of a flawed pipeline, calculated following a fitness for service methodology. There is an increasing risk of subcritical crack growth in H_2 as the hardness of base metal and welds increases. This paper analyzes where zones with high hardness and susceptible microstructures are expected in existing pipelines.

***Corresponding author: Mariano A. Kappes**, Instituto Sabato, UNSAM/CNEA, Av. General Paz 1499, San Martín, Buenos Aires B1650KNA, Argentina; National Commission of Atomic Energy of Argentina, Av. General Paz 1499, San Martín, Buenos Aires B1650KNA, Argentina; and National Scientific and Technical Research Council, Godoy Cruz, 2290, Buenos Aires C1425FQB, Argentina, E-mail: marianokappes@gmail.com. https://orcid.org/0000-0002-5708-5565

Teresa Perez, Instituto Sabato, UNSAM/CNEA, Av. General Paz 1499, San Martín, Buenos Aires B1650KNA, Argentina; and TEP Consultora SRL, Buenos Aires, Argentina

Keywords: design code; hydrogen; integrity; pipelines; testing standard.

Nomenclature

API	American Petroleum Institute
ASME	American Society of Mechanical Engineers
ASTM	American Society for Testing and Materials
b	co-volume constant
B	thickness of fracture mechanics test specimen
C_0	concentration of dissolved atomic hydrogen
CE	carbon equivalent
CMOD	crack-mouth opening displacement
CTOD	crack-tip opening displacement
D	pipeline external diameter
da/dN	rate of crack growth per cycle during fatigue
D_L	hydrogen diffusion coefficient in interstitial sites
E_W	longitudinal joint factor
E	Young's modulus
EIGA	European Industrial Gases Association
f	hydrogen fugacity
F	pipeline design factor (it accounts for proximity of pipeline to roads, highways, rails, streets, and buildings)
FCGR	fatigue crack growth rate
HAZ	heat affected zone
HB	hardness in Brinell scale
HE	hydrogen embrittlement
HEDE	hydrogen enhanced decohesion
HELP	hydrogen enhanced localized plasticity
H_f	material performance factor in gaseous H_2
HIC	hydrogen induced cracking
HRB	Hardness in Rockwell B scale
HRC	Hardness in Rockwell C scale
HTHA	temperature hydrogen attack
HV	hardness in Vickers scale
IGEM	Institution of Gas Engineers and Managers
ILI	in-line inspection, a non-destructive technology for detecting flaws in pipelines
ISO	International Organization for Standardization
J	a mathematical expression that characterizes the stress-strain field around the crack tip
J_H	hydrogen flux

J_{IC}	value of J at the onset of crack extension
K	stress intensity factor
$K_{I\ app}$	applied K in a constant load or displacement test
K_{IC}	critical stress intensity factor for crack propagation in air
K_{IH}	critical stress intensity factor for crack propagation in hydrogen, measured under rising displacement
K_{max}	maximum stress intensity during fatigue
K_{min}	minimum stress intensity during fatigue
K_r	toughness ratio
K_{TH}	crack arrest stress intensity factor, measured under constant load or displacement
L_r	load ratio
MAOP	maximum allowable operating pressure
N	number of stress cycles to failure during fatigue
P	pipeline operating pressure
P_{fail}	pipeline failure pressure
pH_2	partial pressure of hydrogen
PSL	product specification level
PWHT	post weld heat treatment
R_{ig}	universal gas constant
$R = K_{min}/K_{max}$	stress intensity factor ratio during fatigue
RA	reduction in area
S	Sieverts law coefficient
SMYS	specified minimum yield stress
SPT	small punch test
S_y	yield strength
T	absolute temperature
t	thickness of the pipe or vessel wall
T_f	temperature derating factor
UTS	ultimate tensile strength
δ_{IC}	value of CTOD at the onset of crack extension
$\Delta K = K_{max} - K_{min}$	stress intensity factor range during fatigue
ΔK_0	fatigue crack growth threshold
ν	Poisson ratio
σ_h	hoop stress
Φ	hydrogen permeability
σ_{ref}	reference stress

1 Introduction

Climate change concern is the main driving force to consider hydrogen as an energy carrier (Stetson et al. 2015). Hydrogen is not readily available as H_2 in nature; therefore, energy must be expended to produce it, which can then be partially recovered at the point of use. An envisioned hydrogen economy requires reliable technological devices for producing, storing, transporting, and converting hydrogen to heat, electricity, and useful chemicals. Alternatives for transporting hydrogen include vessels filled with gas or liquid hydrogen mounted on trucks, freight trains or ships, and hydrogen gas pipelines. Currently, around 2000 miles of carbon and low alloy steel dedicated hydrogen pipelines exist in Europe and the United States (ASME B31.12 2019; Gerboni 2016; Rawls and Adams 2012), most of them operated by industrial gas companies.

The mature natural gas network present in many countries includes gathering lines that transport gas from the well to central collecting points, transmission lines to transport the gas at high pressure through long distances, and distribution lines, which operate at lower pressure and connect consumers to the network. There are around 300,000 miles of existing transmission pipelines in the United States alone (Coburn 2020). The estimated construction cost of natural gas pipelines, including materials, labor, right of way and miscellaneous, is around 1.5 million $/mile for a 20” diameter pipeline (Parker 2004), with costs corrected for inflation. The cost of a dedicated H_2 transmission pipeline can be higher than this number considering stricter requirements on materials and welding procedures (ASME B31.12 2019). Therefore, there is a large economic driving force for transporting H_2 or blends in the existing natural gas network. Nevertheless, the use of an infrastructure originally designed for natural gas to transport hydrogen or blends presents a challenge in terms of integrity, since new damage mechanisms can be introduced and/or the kinetics of existing ones can be modified. H_2 can dissociate and enter the metallic network under the operating conditions in pipelines. Atomic hydrogen introduced into the metal lattice can cause hydrogen embrittlement (HE). HE involves changes in the mechanical properties of steels with possible subcritical crack propagation. Previously commented aspects mean costs and pro and cons to consider in each case.

Blending H_2 in natural gas pipelines not only takes advantage of the existing infrastructure but also allows the partial decarbonization of natural gas. It can be considered as an intermediate stage on the path to a hydrogen economy. A blend is characterized by the volume percentage of H_2 in the mixture (equivalent to molar percentage, assuming ideal gas behavior), or alternatively by the partial pressure of H_2 (pH_2) in the mixture. Several technical and economic difficulties must be surmounted prior to blending H_2 in an existing natural gas network, as reviewed elsewhere (Melaina et al. 2013), for example, H_2 can more easily permeate through polymeric gaskets and pipes used in distribution networks. Additionally, H_2 has ⅓ of natural gas energy density, so it decreases the heating value of the mixture; it has a poor flame visibility, higher volume leakage rate than methane and higher ignition probability (IGEM 2021). The focus of this review paper is on the HE of carbon and low alloy steels and their welds used for transmission pipelines.

The service experience on the ~2000 miles of existing hydrogen pipelines is good, which is related to both the low mechanical resistance of the commonly used steels (API 5L X52 and lower grades, like ASTM A 106 Grade B) and the low allowable hoop stress (EIGA 2014; Rawls and Adams 2012), limited to 30%–50% of specified minimum yield stress (SMYS). A couple of failures of hydrogen pipelines in service are described by Thompson and Bernstein (1977). On the other hand, higher grades can be present in natural gas transmission pipelines, depending on the construction year. In fact, grade X60 was introduced in 1966, grade X70 in 1973 (Kiefner and Trench 2001). Hoop stress can be up to 80% of SMYS, depending on pipeline location (ASME B31.8 2010). Most existing natural gas pipelines have more than 40 years of service; for example, in the US, about 43% of the 300,000 miles of existing pipeline were built before 1970 (Clark et al. 2005).

Using the existing natural gas transmission pipelines for blends or H_2 transport is not a new idea. Between 1974 and 1986, the United States Department of Energy financed research programs at the Sandia and Battelle laboratories (Hoover et al. 1981; Holbrook et al. 1982, 1984, 1986). The major effects of H_2 on pipeline steels identified in those programs were the higher fatigue crack growth rate (FCGR), lower fracture toughness in gaseous hydrogen and subcritical crack propagation near welds. These conclusions are still valid today and they are reflected in the requirements included in codes such as ASME B31.12 (2019), applicable to the design of H_2 pipelines.

The first part of this review summarizes the metallurgical evolution of pipeline steels, the laws that control the absorption and diffusion of hydrogen in steels and relevant hydrogen damage mechanisms. Standardized tests applicable to the evaluation of the hydrogen effect on mechanical properties are presented and outstanding results are summarized. The main differences in industry rules and regulations for hydrogen versus natural gas transport are detailed. ASME B31.12 (2019) code applies to pipelines containing more than 10% H_2 (by volume). Applying this code to an existing pipeline for leaner H_2 blends transport might be overconservative, too expensive, and unfeasible. Previous international experience on blending and conversion of natural gas pipelines for hydrogen transport is analyzed. Procedures for assuring reliable transport of blends based on fracture mechanics assessments are presented. The paper concludes with a critical discussion, where the effect of the decrease of fracture toughness in hydrogen on the failure pressure of the pipeline is calculated. Hardness is proposed as a screening tool for hydrogen compatibility, and it is discussed where excessive hardness might be expected in an existing pipeline. For informative purposes, correlations between ultimate tensile strength (UTS) and hardness in different scales are presented in Appendix A.

2 Pipeline steels

Minimum technical requirements for pipeline steels are listed in international publications, such as API Specification 5L (API 5L 2018) or (ISO 3183 2019). Specifications for pipeline steels currently used for natural gas transmission are carbon contents up to 0.28 wt% and manganese up to 1.8 wt%, although actual contents in modern pipelines are typically much lower. The limits depend on the grade SMYS, the product specification level (PSL) and the manufacturing process (i.e., welded pipe or seamless). Current SMYS of pipelines ranges from 175 MPa (25 ksi) to 830 MPa (120 ksi). SMYS is indicated in the grade name, for example, an API 5L X65 has a yield strength (S_y) greater or equal to 65 ksi. In the corresponding ISO standard, SMYS is indicated in the steel grade in MPa units, for instance, the equivalent grade to API 5L X65 would be L450. API 5L sets two different product specification levels (PSL 1 and PSL 2). PSL 2 pipes have stricter requirements than PSL 1 pipes, like both minimum and *maximum* levels for the actual S_y and ultimate tensile strength (UTS), limits on the carbon equivalent (CE) and lower allowable contents of carbon, sulfur and phosphorous. They also have requirements on minimum energy absorbed in Charpy impact tests of base metal, heat affected zones (HAZ) and welds (for welded pipes). For PSL 2 pipes, letters after the SMYS indicate the delivery condition, as rolled, normalized, thermomechanically rolled, quenched and tempered, etc. For example, an API 5L X65Q is delivered in the quenched and tempered condition.

Weldability is a key property for pipeline steels because they are longitudinally or spirally welded in pipe mills and girth welded in the field. In modern steels, the weldability is controlled by reducing the carbon content while maintaining the strength levels with the introduction of alloying elements such as Cr and Mo and very low additions (less than 0.1 wt%) of Nb, Ti and V (Villalobos et al. 2018). Hence, modern pipeline steels were christened “microalloyed” steels. Those elements and a careful control of variables during subsequent thermomechanical and heat treatment processes allow obtaining grain size reduction, microstructure refinement and precipitation hardening (Villalobos et al. 2018). Steels of desired strength, toughness, ductility, and weldability are produced using these technologies. The effect of different alloying elements on the weldability is evaluated using the carbon equivalent (CE) expressions (API 5L 2018):

$$CE_{IIW} = C + \frac{Mn}{6} + \frac{Cr + Mo + V}{5} + \frac{Ni + Cu}{15} \text{ for } C > 0.12\% \quad (1)$$

$$CE_{Pcm} = C + \frac{Si}{30} + \frac{Mn + Cu + Cr}{20} + \frac{Ni}{60} + \frac{Mo}{15} + \frac{V}{10} + 5B, \text{ for } C \le 0.12\% \quad (2)$$

Equation (1) applies to C–Mn and Equation (2) to microalloyed steels. For API 5L PSL 2 pipes, $CE_{Pcm} \le 0.25$ or $CE_{IIW} \le 0.43$.

With a larger CE, a higher hardness and fresh martensite might be present in the HAZ. Depending on the CE and the material thickness, preheating, stricter control of welding variables and, eventually, post weld heat treatments (PWHT) might be required to temper the HAZ and assuring an adequate performance. Those steps increase the total fabrication cost and are not always feasible in the field.

The decades where the growth rate in the transmission pipeline network was largest (Figure 1) (Clark et al. 2005; Leis 2015), coincide with the deployment of several key technologies that improved the microstructure and properties of pipeline steels, like sulfide shape control with calcium and rare earths (Banks and Gladman 1979), microalloying additions, continuous casting, and controlled rolling (Clark et al. 2005). Hence, "modern" and "vintage" steels coexist in the existing transmission natural gas network. Modern pipelines have lower carbon and CE than vintage or C–Mn pipelines of the same grade and therefore a smaller hardness is expected in the HAZ. Additionally, just in 2000 (Kiefner and Trench 2001) a minimum level of absorbed energy in impact testing was made mandatory in API 5L Specification for PSL 2 pipes. Consequently, the steels in most existing natural gas pipelines have not ever been impact tested.

3 Absorption and dissolution of hydrogen in carbon and low-alloy steels

Unlike methane, the main component of natural gas, H_2 can dissociate and atomic hydrogen can dissolve as an interstitial in steels. The equilibrium concentration (C_0) of atomic hydrogen in pure iron in contact with H_2 at atmospheric pressure (1.013 bar) can be estimated with the following equation, by Kiuchi and McLellan (1983), valid between 0 and 90 °C:

$$\ln\left(T^{7/4}C_0\right) = -\frac{3120 \pm 90}{T} + (3.21 \pm 0.32) \quad (3)$$

where T is temperature in K and C_0 is the atomic fraction. This equation predicts $C_0 = 5.9 \times 10^{-4}$ ppm mass at 25 °C, for H_2 at atmospheric pressure. H occupies tetrahedral interstitial sites in the ferritic lattice (α phase) (Kiuchi and McLellan 1983).

Sievert's law (Xu 2012) predicts that H solubility (C_0) increases with the square root of H_2 partial pressure, pH_2:

$$C_0 = S\sqrt{pH_2} \quad (4)$$

where S is the Sieverts law coefficient. The equations above highlight that from a materials perspective, pH_2 in the blend is a much more representative parameter than hydrogen volume (or molar) concentration in the blend, unless the later magnitude is accompanied by operating pressure. For example, at 100 bar (10 MPa), a pressure representative of the upper expected values for the maximum allowable operating pressures (MAOP) of buried natural gas pipelines, and a H_2 concentration of 10% (pH_2 = 10 bar), using Equations (3) and (4), C_0 results equal to 1.86×10^{-3} ppm mass at 25 °C.

For buried pipelines, cathodic electrochemical reactions from cathodic protection or corrosion processes provide additional hydrogen entry paths (Shipilov and Le May 2006). The applied potential, water solution composition and oxides or deposits present on the steel surface affect C_0. C_0 can be estimated with hydrogen permeation data, as recently reviewed by Turnbull (2015). For pipeline steels cathodically polarized in solutions that simulate Canadian groundwater (referred to as NS4 solution), hydrogen concentration on the charging surface is on the order of 1×10^{-3} ppm mass according to several studies (Chen et al. 2000; He et al. 2004; Ma et al. 2021). Groeneveld and Elsea (1974) reported C_0 values ranging from 1×10^{-3} to 1×10^{-2} ppm mass for hydrogen permeation in soils and ground waters under cathodic protection. Sour corrosion is one of the most severe conditions for hydrogen absorption (Perez 2013), promoting sulfide stress cracking, a form of HE, on a susceptible material if certain critical hydrogen concentration and tensile stress levels are present. For acidified brines bubbled with H_2S commonly used for simulated sour fluids, C_0 depends mainly on H_2S partial pressure and pH. Reported values range from 0.02 to 0.1 ppm (Asahi et al. 1994; Cancio et al. 2014; Hara et al. 2004; Kappes et al. 2012) at open circuit conditions.

Previously mentioned values referred exclusively to the hydrogen concentration in interstitial sites. It is well known that hydrogen interacts with defects in steels, such as vacancies, dislocations, and grains and second phase boundaries, leading to H trapping (Turnbull 2015). Trapped

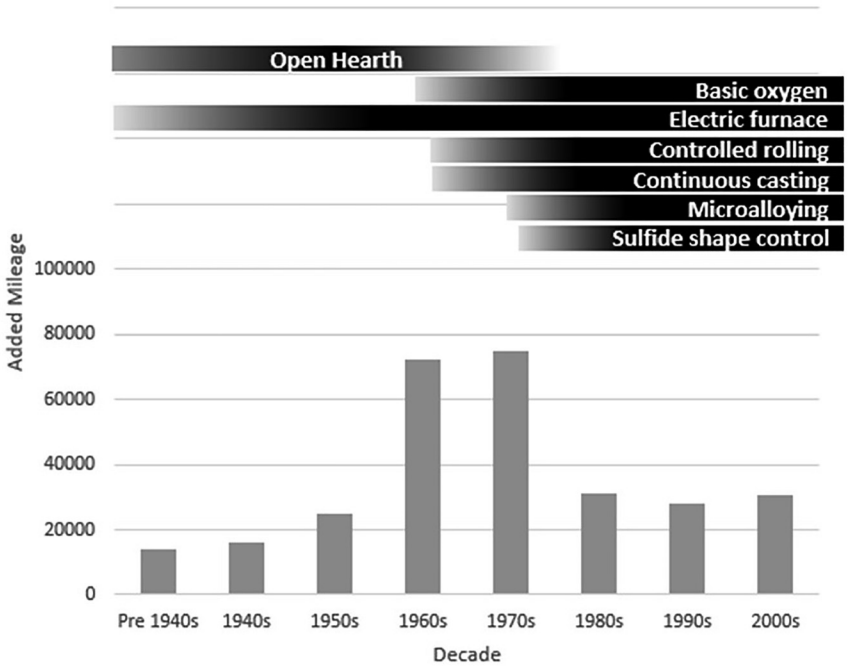

Figure 1: Mileage of natural gas transmission pipeline added to the US network by decade of construction, showing major breakthroughs in steelmaking technology (adapted from Clark et al. 2005; Leis 2015).

hydrogen concentration scales with C_0, it is dependent on the population of defects in the steel, and in most cases, equilibrium between both populations can be assumed (Oriani 1970). Total hydrogen concentration includes trapped and interstitial populations and depends on both environmental parameters and steel microstructure.

4 Hydrogen diffusion

Once dissolved in the metal lattice, atomic hydrogen can move macroscopic distances, even at room temperature. The diffusion coefficient of hydrogen in the ferritic lattice (*a*) at 25 °C is $D_L = 7.27 \times 10^{-5}$ cm^2/s (Turnbull 2012). This value is more than 10 orders of magnitude larger than the diffusion coefficient for carbon (*C*), also dissolved as an interstitial in steel (Porter and Easterling 1992). D_L controls hydrogen transport at the steady state. The high D_L at room temperature allows the movement of atomic H and its interaction with tensile stress fields, promoting crack propagation, and the permeability through metallic components. Hydrogen effects on crack propagation will be discussed in upcoming sections. Permeation implies that at steady state a flux of hydrogen evolves from vessels and pipes filled with H_2, on top of possible additional leakage through apertures like pinholes, through-wall flaws or unsealed threads.

On a pressurized pipe or vessel, H_2 dissociates on the high-pressure surface, dissolves in the steel matrix, and diffuses down the concentration gradient, recombining at the exit surface. Hence, the transport of hydrogen involves both surface reactions and diffusion down a concentration gradient. Considering diffusion is the slow step, Fick's first law can be used to estimate hydrogen flux across the wall at steady state. When the concentration of hydrogen on the exit surface is negligible, the hydrogen flux, J_H, will be maximum for a given internal pressure and temperature. Using Fick's first law with D_L, and introducing Sievert's law (Equation (4)),

$$J_H = \frac{D_L C_0}{t} = \frac{D_L S \sqrt{\mathrm{pH_2}}}{t} \tag{5}$$

where t is the thickness of the pipe or vessel wall. Permeability (Φ) is defined as the product of diffusivity and solubility at unit pressure, and it increases with temperature because both D_L and S increase with T (Schefer et al. 2006):

$$\Phi = D_L S = \frac{J_H t}{\sqrt{\mathrm{pH_2}}} \tag{6}$$

At high pressure, pH_2 is replaced by fugacity (*f*) in Equations (5) and (6), to account for its non-ideal behavior (Schefer et al. 2006). Fugacity (*f*) can be estimated according to:

$$f = \mathrm{pH_2} e^{\frac{\mathrm{pH_2} b}{R_{ig} T}} \tag{7}$$

where R_{ig} is the universal gas constant and b is the "co-volume" constant. Constant b describes the non-ideal behavior of hydrogen and for temperatures between 200 and 350 K and pressures up to 160 MPa, its value is 15.5 cm^3/mol (Schefer et al. 2006).

If oxides or coatings are present on either surface, they might decrease the rate of hydrogen absorption or

desorption surface reactions, and the resulting flux will be smaller. Furthermore, carbon and other alloying elements present in the steel can decrease the hydrogen permeability (Chalfoun et al. 2022; Gadgeel and Johnson 1979). Therefore, Equation (5) gives conservative estimates for the rate of hydrogen permeation as a function of hydrogen pressure, temperature, and wall thickness. For example, at pH_2 = 100 bar (10 MPa) and for t = 5 mm at room temperature, the permeation loss is 4×10^{-3} cm^3 H_2 @ STP/(m^2 s), where STP is standard temperature and pressure. Hence, considering the small losses due to permeation, the main effect of the high D_L is related to H transport to stressed regions, affecting mechanical properties as discussed in upcoming sections.

5 Hydrogen damage mechanisms in transmission pipelines

Once absorbed by the steel lattice, H can give rise to different degradation mechanisms, namely, high temperature hydrogen attack (HTHA), hydrogen induced cracking (HIC) and hydrogen embrittlement (HE). Temperature and hydrogen activity or fugacity in the environment are the most important variables for the occurrence of each mechanism. There is still confusion in the nomenclature of these mechanisms, even in specialized technical literature. This review adheres to the definitions adopted by the standards and recommended practices most used by the industries that suffer from those problems (API RP 941 2016; ISO 15156 2015; NACE/ASTM G193 2020; NACE TM0284 2016). HTHA involves the dissolution of carbides and the carbon reaction with dissolved hydrogen to form methane pores, which grow leading to fissures and cracks. It occurs in components exposed to gaseous hydrogen or hydrogen mixtures at temperatures above 200 °C (API RP 941 2016). Hence, it is not an expected mechanism for buried transmission pipelines. HIC and blistering occur at or near room temperature and involve the recombination of hydrogen at matrix/inclusions interfaces to produce H_2. This produces pressurization of the interface and promotes crack propagation. Crack propagation requires a high pressure at this cavity, which is in turn controlled by dissolved hydrogen concentration. The minimum concentration of hydrogen in interstitial sites for HIC occurrence depends on steel microstructure, although C_0 > 0.02 ppm can be cited as a reference value (Hara et al. 2004). Hence, considering the expected hydrogen concentration in a buried pipeline transporting natural gas or blends quoted before, HIC is not an expected damage mechanism (Chen et al. 2000). In practice, the required high hydrogen concentration for HIC is typically encountered during corrosion of steels in H_2S containing solutions (Martin and Sofronis 2022).

The third damage mechanism, and the only one expected for the application under study, is HE, also known as hydrogen assisted cracking. It causes a decrease in the ductility and fracture toughness of the material and can lead to subcritical crack propagation under static loads or displacements and to an increase in FCGR if loads fluctuate over time. Unlike the previous mechanisms, crack nucleation and propagation require applied and/or residual tensile stresses. For carbon and low alloy steels, the risk of failure by HE is maximum near room temperature. Depending on the material strength level and microstructure, failures can occur in diverse environments present in different industries. HE involves interaction of hydrogen with the hydrostatic stress field present at the crack tip, where the stress level can be well above the S_y. Hydrogen promotes crack propagation under static or cyclic loads by decohesion (HEDE, hydrogen enhanced decohesion), localized crack tip plasticity (HELP, hydrogen enhanced localized plasticity) or a synergistic mechanism (Bouledroua et al. 2020; Gangloff 2003; Robertson et al. 2005), which is still under debate in the literature.

The most effective way to prevent HE failure is by an adequate materials selection, controlling strength and microstructure. International standards and codes that rule materials selection processes impose stricter limits on strength level as the hydrogen activity or fugacity in the environment increases. For example, for buried pipelines under cathodic protection, ISO 15589-1 (2015) standard recommends to “document or determine experimentally” the lowest allowable cathodic protection potential when S_y of base metal is above 550 MPa (80 ksi). The aim is to prevent HE due to the increased rate of hydrogen production as the cathodic potential decreases. Usually, the material hardness (related to strength) is limited to avoid HE. However, it is important to remark that microstructure is key to define the HE material susceptibility. Two materials with different microstructures and the same hardness can have different susceptibilities (Echaniz et al. 1998). For sour service, a limit of 22 HRC is placed on the base metal and 250 HV for welds and HAZ (ISO 15156 2015). For pipeline steels, the strength of API 5L grades used for sour service is limited to 65 ksi or 80 ksi, depending on the H_2S partial pressure and pH of the environment, both of which control the hydrogen activity in the environment. For pipeline steels used for gaseous hydrogen, SMYS is limited to 360 MPa (52 ksi) (EIGA 2014). However, this limit can be increased up to 550 MPa (80 ksi) if the steel grade is qualified for hydrogen service, according to tests to be detailed later in this review (ASME B31.12 2019).

6 Hydrogen embrittlement of pipeline steels in gaseous hydrogen: applicable testing standards and main results

Recent results reported in the literature (Briotett and Ez-Zaki 2018; Meng et al. 2017; Nguyen et al. 2021a; Ronevich and San Marchi 2021; San Marchi and Somerday 2012) indicate that there does not exist a lower threshold for hydrogen partial pressure required for observing HE. In other words, for a transmission pipeline there is not a partial pressure or percentage of hydrogen in the blend below which hydrogen would not be a threat to materials integrity. How these degraded properties affect structural integrity can be assessed with a fracture mechanics-based framework.

Comprehensive reviews on the effect of hydrogen on materials properties were published (Lam et al. 2007; Laureys et al. 2022; Nanninga et al. 2010; San Marchi and Somerday 2012). The main consequences and findings relevant to the application under study are discussed below.

Observed trends can be summarized as follows:

- For a given steel microstructure, an increase in strength decreases ductility and fracture toughness in gaseous hydrogen.
- Within the expected strength range of pipeline steels, the increased FCGR does not exhibit a clear correlation with strength level.
- For pipeline steels, subcritical crack growth in gaseous hydrogen is only expected in exceptionally hard or susceptible microstructures, in practice most likely present in zones that experienced a fast cooling rate from the austenitic field (like the HAZ) or in cold worked zones.

Table 1 presents a non-exhaustive list of standards commonly used for quantifying hydrogen effects on materials properties.

Table 1: Standard test methods commonly used to quantify the effect of gaseous hydrogen in mechanical properties of steels.

H_2 affected property	Standard designation	Summary of test method	Comments
Plastic elongation ratio Reduction in area Ultimate tensile strength	ASTM G142	Smooth or notched specimens are slowly pulled to failure in uniaxial tension in a pressurized, H_2 containing environment	Comparison of properties measured in hydrogen versus a non-embrittling environment (control test, i.e., air typically) allows calculating ratios of reduction in properties and to rank materials behavior in hydrogen
Fracture toughness	ASTM E1820	A fatigue-precracked fractomechanic specimen is loaded at *rising* displacement generating unstable or stable crack propagation. Performed in air or in a pressurized hydrogen containing vessel	Pipeline steels usually exhibit stable crack propagation in air and gaseous hydrogen. In this case, K_{IC} (in air) or K_{IH} (in hydrogen) can be estimated from *J* or CTOD measurement. K_{IC} (K_{IH}) represents the critical stress intensity factor for crack propagation in air (hydrogen)
Crack-arrest stress intensity factor[a]	ASTM E1681	A fatigue-precracked fractomechanic specimen is loaded at *constant* displacement or load while immersed in a hydrogen-containing vessel	Crack propagation might ensue during the test. The test method allows estimation of $K_{TH,}$ the crack arrest stress intensity factor in the presence of hydrogen
Fatigue crack growth rate[a]	ASTM E647	A fatigue-precracked fractomechanic specimen is cyclically loaded at a given frequency, while monitoring crack length	Usually presented as da/dN versus ΔK curves, where da/dN is the crack growth rate per cycle and ΔK is the range in stress intensity factor

[a]Test required by performance-based design method in ASME B31.12 (2019) for qualification of base metal and welding procedures. Measured in pure H_2 at the component design operating pressure.

6.1 Uniaxial tensile tests

Plastic elongation and reduction in area (RA) both quantify the material's capacity to deform plastically. Hydrogen effects are evaluated by the ratios of these properties measured in a hydrogen containing versus a control environment (air, typically). Usually, relative changes in RA are larger than for the rest of the parameters measured during a tensile test (Hoover et al. 1981; Meng et al. 2017; Nguyen et al. 2020a,b). RA is attractive because it does not depend on specimen gauge length, and it can be used for both smooth and notched specimens. The decrease in mechanical properties is dependent on the materials strength level, microstructure, and environmental parameters. Additionally, the

extension rate is also important, and it must be low enough to allow absorption, diffusion, and interaction of hydrogen with defects. For gaseous H_2 tests of smooth specimens, ASTM G142 (2016) suggests 0.002 mm/s, and 0.02 mm/s for notched specimens. However, the standard indicates that a full characterization of hydrogen embrittlement might require tests at higher or lower values.

For smooth specimens, a comprehensive review (San Marchi and Somerday 2012) concluded that S_y and UTS of carbon and low alloy steels typically used for pipelines are similar in H_2 versus air, for pressures ranging between 6.9 and 69 MPa. In contrast, RA in H_2 is reduced up to 50% of the value in air. Hydrogen effects can even take place at very low partial pressure, for example, for 1% H_2 in 10 MPa of methane, RA at the girth weld of an API 5L X70 steel was 52%, versus 70% measured in air (Nguyen et al. 2020a). On the other hand, for the base metal RA in this environment was close to RA in air, a decrease in RA in the base metal was only observed in pure H_2 at 10 MPa. It is likely that the microstructure of the weld increased its susceptibility to hydrogen embrittlement. For tests performed in the H_2 containing environment, secondary cracks were observed in the gauge surface and quasi-cleavage facets in the fracture surface (Nguyen et al. 2020a). On the other hand, the specimens tested in air presented a ductile fracture with small dimples.

Notches increase the sensitivity of the test to hydrogen effect and the relative reductions in RA are larger than those measured for smooth specimens. Reduction of RA of up to 80% in H_2 at 6.9 MPa was reported (Hoover et al. 1981). In notched specimens, hydrogen also decreases the value of UTS (Hoover et al. 1981; Meng et al. 2017; San Marchi and Somerday 2012). For the base metal of API 5L X70 pipeline steel tested in a 1% H_2 in 10 MPa of methane mix, RA decreased by 55% with respect to air values for a notched specimen but RA values were similar for smooth specimens (Nguyen et al. 2020b).

The slow strain rate test is the simplest, fastest, and most affordable test, but it does not allow performing structural integrity assessments. Its usefulness is limited to ranking materials in each environment or ranking the severity of different environments. Michler et al. (2012) presented a correlation between the loss in RA in hydrogen with the reduction in fracture toughness in H_2 for different materials. There are exceptions to this correlation, for instance while RA of an X70 pipeline steel was not affected by 1% H_2 in 10 MPa methane, the fracture toughness, estimated from the critical crack tip opening displacement (CTOD) for crack propagation, was reduced from 205 MPa $m^{1/2}$ to 144 MPa $m^{1/2}$ (Nguyen et al. 2020b, 2021a).

6.2 Fracture mechanics tests

Due to the reduced resistance to crack propagation in H_2 versus air, injecting hydrogen into a natural gas pipeline can decrease the failure pressure depending on the defect size, or alternatively, for a fixed operating pressure, the dimensions of the largest allowable defect decreases. The quantification of these effects is central to the use of natural gas pipelines for transporting H_2 or blends. For welded components, structural integrity assessments require hydrogen affected fracture toughness and hydrogen accelerated FCGR in base metal, weld metal and HAZ. The effect of hydrogen on fracture mechanics properties is studied with specimens with a notch and a fatigue precrack. A challenge of the test specimen machining is that the notch might not be situated exactly in the most susceptible zone of the welded region.

Fracture mechanics fatigue-precracked specimens can be loaded under rising displacement in H_2 or at constant load or displacement (Table 1). Tests under rising displacement allow determining the critical stress intensity factor for crack propagation in hydrogen (K_{IH}). If the material is tested at constant load or displacement, the crack arrest stress intensity factor (K_{TH}) is obtained.

Figure 2 illustrates crack length (a) and stress intensity factor (K) versus time, for both testing alternatives. For high strength steels, as the loading rate decreases (Clark and Landes 1976), K_{IH} approaches K_{TH}. However, for steels with S_y < 900 MPa, $K_{IH} < K_{TH}$ (Nibur et al. 2013). It is proposed that hydrogen assisted fracture in high strength steels is stress controlled, whereas for steels with S_y < 900 MPa it is strain controlled (Nibur et al. 2013). For high strength steels, HEDE mechanism controls the fracture process at the crack tip (Gangloff 2003). For lower strength steels, like pipeline steels, the plasticity accompanying fracture is larger and the sequence of loading and hydrogen absorption is important (Martin et al. 2022). Hydrogen facilitates dislocation motion, which is the basis of the HELP mechanism (Robertson et al. 2015). Notice that in a rising displacement test in hydrogen environment, strain (dislocation motion, microscopically) and hydrogen absorption occur concurrently. For constant displacement tests, first the specimen is loaded and deformed in an inert environment, and then hydrogen is absorbed and saturates the crack tip region after an incubation time (Figure 2). Hence, differences in strain history promote disparities between K_{IH} and K_{TH}. For the base metal of pipelines steels, there is no reported crack propagation in fatigue pre-cracked specimens under constant displacement conditions (Loginow and Phelps 1975; Nibur et al. 2013; Nibur and Somerday 2012; San Marchi and Somerday 2012; Tazedakis et al. 2021; Xu 2012). For those steels, the risk of crack

propagation under constant displacement conditions is limited to welds, HAZ and susceptible microstructures.

6.2.1 Testing methods

6.2.1.1 Fracture toughness measured under rising displacement (K_{IH})

Fracture toughness in air is measured with fatigue pre-cracked specimens (ASTM E1820 2020), loaded to fracture while monitoring load and displacement. The material can present unstable or stable crack propagation. For the first case, the standard allows the calculation of a critical value of fracture toughness, K_{IC}. The expected response for pipeline steels is stable crack propagation; it is characterized by fracture toughness versus crack propagation curve (R-curve), which represents the tearing response of the material. From this curve, the fracture toughness (K_{JIC}) for the onset of crack extension can be obtained, according to (Anderson 2005; ASME BPVC VIII.3 2017):

$$K_{JIC} = \sqrt{\frac{EJ_{IC}}{1-\nu^2}} \tag{8}$$

where E is the Young's modulus and ν is the Poisson ratio. The "J" subscript indicates that fracture toughness is obtained from the J integral, a mathematical expression that characterizes the stress–strain field around the crack tip. J_{IC} characterizes crack-extension resistance near the onset of stable crack extension. Alternatively, the toughness of the material can be evaluated by monitoring the crack-tip opening displacement (CTOD), and the equivalent $K_{\delta IC}$ is obtained according to (ASME BPVC VIII.3 2017)

$$K_{\delta IC} = \sqrt{\delta_{IC} E S_y} \tag{9}$$

where δ_{IC} is the value of CTOD at the onset of crack extension.

To characterize the effect of hydrogen, the tests are performed with the specimen immersed in a H_2 pressurized autoclave. Loading rate must be slow enough to fully allow H

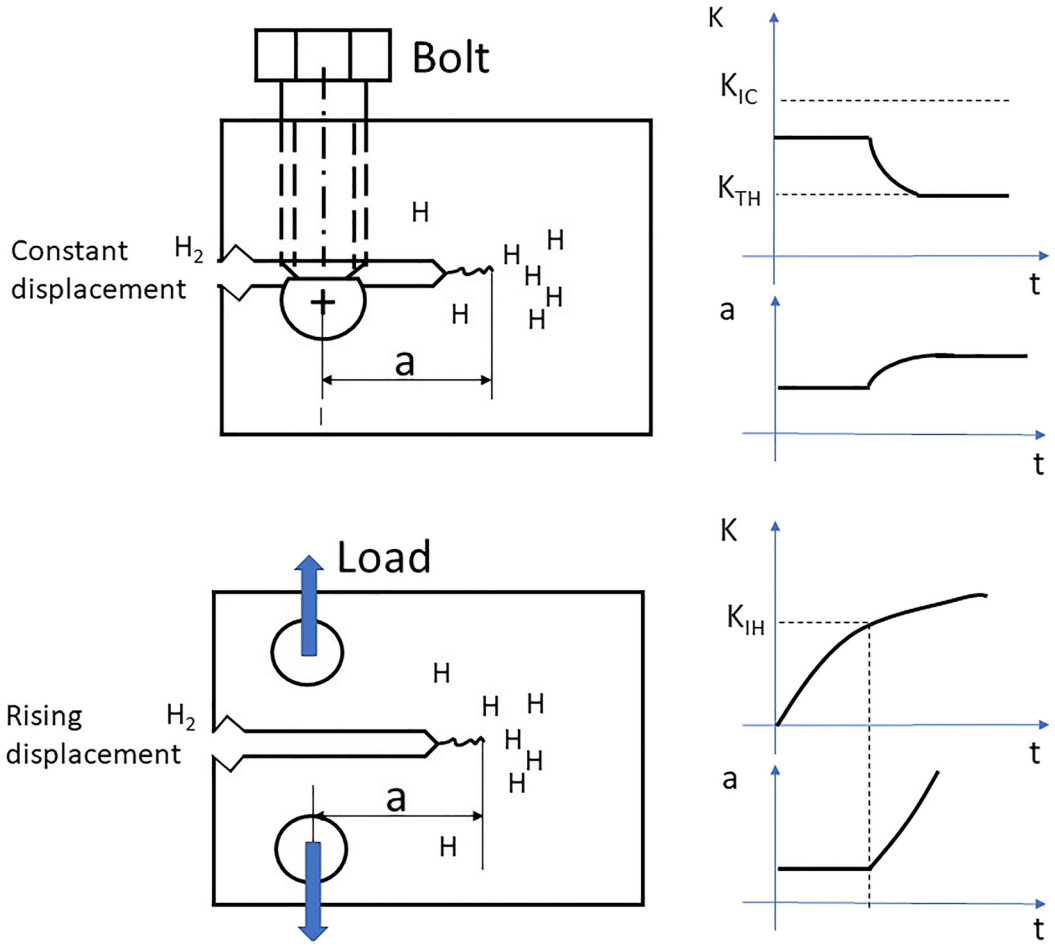

Figure 2: Schematic dependences of K and crack length (a) versus time for constant and rising displacement tests, adapted from Nibur et al. (2013). The incubation time for crack propagation under constant displacement is related to absorption and diffusion of H to the crack tip.

absorption and H embrittlement phenomena (Nibur and Somerday 2012). The measured parameter is K_{IH}, where the "*H*" means that the test was performed in hydrogen. The "*J*" and "*δ*" subscripts (Equations (8) and (9)) are often omitted.

6.2.1.2 Tests under constant load or displacement (K_{TH})

The ASTM E1681 (2020) standard covers the determination of the environment-assisted cracking threshold stress intensity factor parameters, at constant load or displacement. The specimen (Figure 3) is loaded below its K_{IC} in air (or K_{JIC} or $K_{\delta IC}$, if applicable) and immersed in an environment containing H_2 where it is held under constant load or displacement for a given amount of time. During this period, hydrogen diffuses into the specimen and crack propagation might (Figure 2) or might not occur. The threshold stress-intensity factor for sustained-load cracking or crack arrest stress intensity factor (K_{TH}) is defined as the maximum applied $K_{I\ app}$ that did not cause crack propagation at constant load, or the minimum $K_{I\ app}$ that showed evidence of crack propagation under constant displacement (ASTM E1681-03 2020). Notice that under constant displacement, $K_{I\ app}$ decreases when the crack advances (Figure 2). For both types of tests, testing time is a key variable, and must be not less than 1000 h for pipeline steels in gaseous hydrogen, according to article KD 10 in ASME BPVC VIII.3 (2017). If the plane strain condition, $B > 2.5\ (K_{TH}/S_y)^2$ is not fulfilled, the obtained K_{TH} is thickness dependent. In that case, *B* (test specimen thickness) must be not less than 85% of the thickness of the component under analysis (ASME BPVC VIII.3 2017).

Constant load tests are performed in a rigid fixture, where a beam with a notch and a fatigue precrack is loaded with deadweight (Figure 3). The applied stress intensity factor, $K_{I\ app}$, can be estimated from specimen geometry, crack length, applied weight and the length of the moment arm, *L*, following expressions in ASTM E 1681 (2020). For constant displacement tests, a compact specimen with a fatigue precrack and a crack mouth opening displacement (CMOD) gage is loaded to a fixed CMOD, by tightening the bolt against a flattened pin (Figure 3). $K_{I\ app}$ can be estimated from specimen geometry, crack length and CMOD (ASTM E 1681 2020).

Test specimens must be mechanically loaded under a controlled atmosphere to prevent crack tip oxidation (Nibur et al. 2013; ASME BPVC VIII.3 2017). A major advantage of bolt loaded specimens is that several specimens can be arranged in a single H_2 pressurized autoclave. $K_{I\ app}$ should be at least 1.5 times greater than the expected K_{TH} value (ASME BPVC VIII.3 2017) for constant displacement tests. If the crack propagates during the test, $K_{I\ app}$ decreases and the crack arrests when $K_{I\ app} = K_{TH}$. At the end of the test, the specimen is broken to expose the crack, its growth in the environment is assessed with a scanning electron microscope and K_{TH} can be estimated (ASTM E 1681 2020; ASME BPVC VIII.3 2017). Notice that ASTM E1681 (2020) requires some crack extension after 1000 h for a valid K_{TH} at constant displacement. The KD 10 article (ASME BPVC VIII.3 2017), on the other hand, allows setting K_{TH} to 0.5 K_{app} if the crack did not propagate (or propagated less than 0.25 mm) in the test.

6.2.2 Results

6.2.2.1 K_{IH} in base metal

Fracture toughness in H_2 (K_{IH}) decreases with an increase in H_2 partial pressure (Briottet and Ez-Zaki 2018; Gutierrez-Solana and Elices 1982; Robinson and Stoltz 1981) (Figure 4), and with steel strength (Nibur et al. 2013; San Marchi and Somerday 2012). Figure 4 has a logarithmic scale on the pressure axis to highlight the aggressive effects of H_2 even at very low partial pressure. Results obtained in methane + H_2

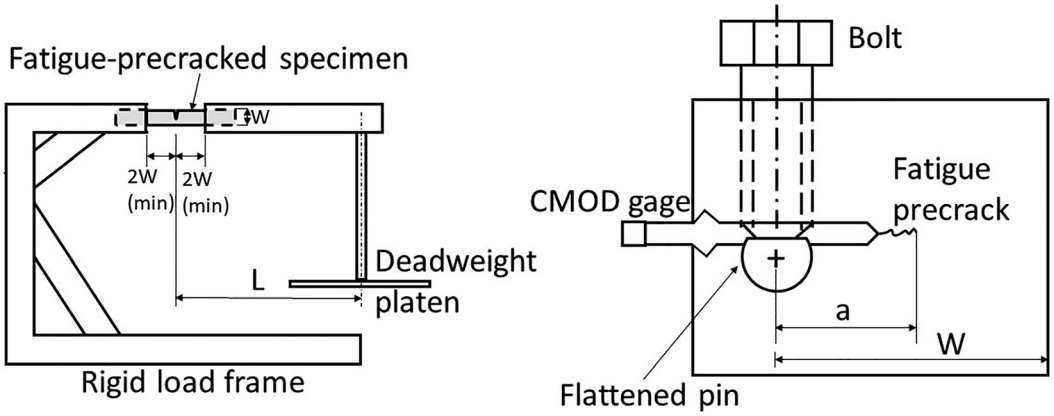

Figure 3: Constant load (left) and constant displacement (right) test arrangements for measurement of K_{TH} (ASTM E1681 2020).

or nitrogen + H_2 mixtures for API 5L X70 (Briotett and Ez-Zaki 2018; Nguyen et al. 2021a) or X52 (Ronevich and San Marchi 2021) conclude that K_{IH} can range from 47% to 70% of K_{IC}, even for very low H_2 partial pressures. Both methane and nitrogen are considered inert gases with respect to crack propagation (Holbrook et al. 2012). Those low H_2 partial pressures represent H_2 percentages ranging from 1% to 6% in the blend if total pressure is 10 MPa. Hence, for transmission pipelines there does not exist a blending percentage or hydrogen partial pressure threshold below which the HE effect is negligible.

6.2.2.2 K_{IH} in welds and HAZ

Base metal and welding filler chemical compositions, and welding procedure control the strength and microstructure of the weld and heat affected zone (HAZ). In practice, the microstructure and strength of welds and HAZs are indirectly inferred from hardness or microhardness profiles. Based on different studies, the K_{IH} at the HAZ might be smaller than in welds and base metal, depending on welding procedure and base metal composition.

For an API 5L X60 in 6.9 MPa H_2, the fused zone of submerged arc welds (SAW) had a K_{IH} (obtained from J measurements) close to the one measured on the base metal (104 MPa $m^{1/2}$) (Hoover et al. 1981). Similar results were recently published for X52, X65 and X100 (Ronevich et al. 2021) in 21 MPa H_2. On the other hand, subcritical crack propagation was detected during the J measurement in 6.9 MPa H_2 when the crack grew through the HAZ of the SAW of an API 5L X60 (Hoover et al. 1981), making it impossible to obtain a reliable K_{IH} value. The HAZ had a hardness value of around 96 to 98 HRB (corresponds to UTS between 705 and 750 MPa), versus 91 HRB for the base metal (620 MPa). Measurements on the HAZ of electric-resistance welds (ERW) of API 5L X42 steel revealed a K_{IH} of 48 MPa $m^{1/2}$ in 6.9 MPa H_2, versus 107 MPa $m^{1/2}$ for the base metal (Cialone and Holbrook 1988; Holbrook et al. 1982). Hardness of base metal and HAZ were 81 and 99 HRB (505 MPa and 785 MPa), respectively. More recently, Martin et al. (2022) reported 86 MPa $m^{1/2}$ in 10 MPa H_2, for the HAZ of a microalloyed API 5L X70 steel, versus 95 MPa $m^{1/2}$ for the base metal.

6.2.2.3 K_{TH} in base metal

In gaseous H_2, cracks on fatigue pre-cracked specimens machined from the base metal of pipeline steels do not propagate at constant load or displacement. Loginow and Phelps (1975) performed bolt loaded (Figure 3 right) constant displacement tests on carbon and low alloy steels with S_y ranging from 290 to 1055 MPa (42–153 ksi), at H_2 pressures up to 97 MPa (14 ksi). K_{TH} values decreased with an increase in S_y and H_2 pressure. However, subcritical crack propagation was not observed in steels with S_y < 587 MPa (85 ksi), with a UTS of 689 MPa (100 ksi). Cialone and Holbrook (1988) did not detect subcritical crack growth in an API 5L X70 steel (SMYS = 480 MPa), with 98 HRB, at constant CMOD in a 6.9 MPa blend containing 40% CH_4 + 60% H_2.

According to ASME B31.12 (2019), the performance-based method (discussed in item 6 in this manuscript) requires K_{TH} ≥ 50 ksi.$in^{1/2}$ (55 MPa $m^{1/2}$). When there is no crack propagation in CMOD tests at the end of the test, article KD 10

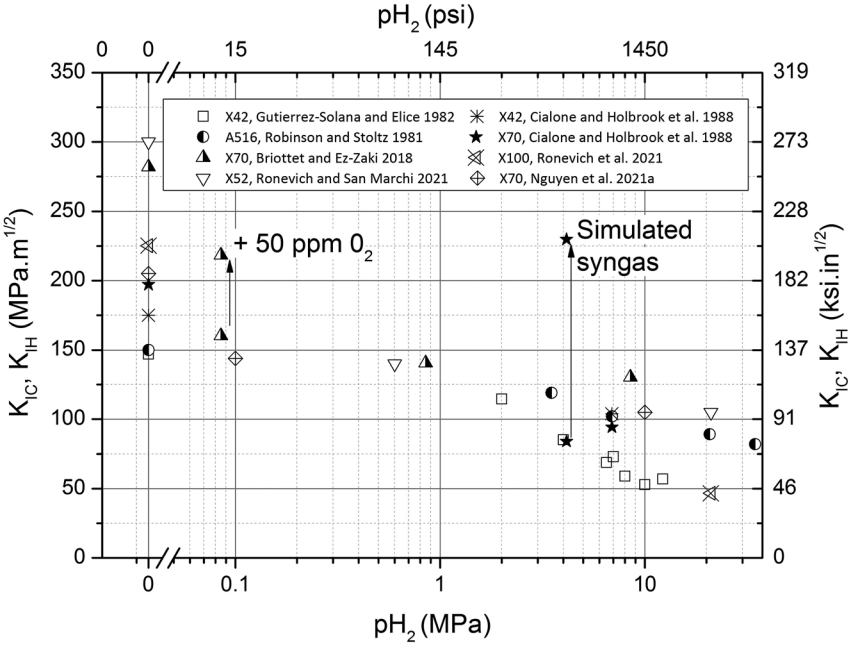

Figure 4: H_2 effect on steel fracture toughness, for various API 5L grades and A516 steel [S_y = 345 MPa (50 ksi)], showing the effect of partial pressure and inhibitors. Simulated syngas: 60% H_2, 24% CO, and 16% CH_4, at a total pressure of 6.9 MPa.

in ASME BPVC VIII.3 2017 (2017) allows to set $K_{TH} = K_{I\ app}/2$. It might be questionable to estimate an arrest threshold for a crack that never propagated. It is interpreted that dividing the $K_{I\ app}$ by 2 would yield a conservative K_{TH} value when there is no crack propagation, but the support for this is not explained in the code. Hence, for qualifying low strength pipeline steels (S_y < 600 MPa) for hydrogen service $K_{I\ app}$ was initially set at 110 MPa $m^{1/2}$ (Tazedakis et al. 2021). Recently, microalloyed API 5L X60, X65, and X70 and their welds were qualified in pure H_2 at 8 MPa (Tazedakis et al. 2021). Those steels obtained with modern steel making techniques have C < 0.07 wt% and CE_{Pcm} < 0.17 wt%. Notice that this result for modern steels cannot be directly extrapolated to similar grades in existing natural gas pipelines.

6.2.2.4 K_{TH} in welds, HAZ and hardened microstructures

Crack propagation at constant CMOD was reported for a water quenched API 5L X42 steel in a 6.9 MPa blend containing 40% CH_4 + 60% H_2. The obtained microstructure had very high hardness (38 HRC, UTS 1180 MPa approximately) and might be representative of the fresh martensite potentially present in hard spots of pipelines (Cialone and Holbrook 1988). However, the corresponding K_{TH} value was not informed. Holbrook et al. (1982) reported crack growth in the HAZ of an ERW API 5L X42 steel (with %C = 0.26 and CE_{IIW} = 0.41), in a constant CMOD test in H_2 at 6.9 MPa (1000 psi). $K_{I\ app}$ was 77 MPa $m^{1/2}$, but the K_{TH} was not reported. It is remarkable that in tests where subcritical crack propagation was observed (Holbrook et al. 1982; Hoover et al. 1981) the hardness in the HAZ reached values of 98 HRB, which corresponds to a UTS on the order of 750 MPa (109 ksi). Recently (Xu 2012), subcritical crack growth was also measured in the HAZ of an API 5L X80 steels tested at constant CMOD in 31 MPa H_2. The crack extended along a zone with a very high hardness, around 42 HRC (UTS 1340 MPa).

The evidence available in the literature suggests that 98 HRB (equivalent to 228 HV) or 750 MPa for UTS might be adopted as hardness and strength thresholds for subcritical crack propagation at constant CMOD in gaseous H_2. For pipeline steels, those hardness and strength values might be expected in the HAZ, for example. Engineering codes and standards for hydrogen transport in pipelines have strict limits on hardness and strength of base metal, welds and HAZ, in line with the results presented in this section. For example, the ASME B31.12 code limits UTS of base metal and welds to 110 ksi (760 MPa) for the performance-based method and 100 ksi (690 MPa) for the prescriptive design method (see item 6 in this manuscript). According to the performance-based method, K_{TH} must be measured following article KD-10 in ASME BPVC VIII.3 (2017). Tests are conducted according to ASTM E1681 (2000) in pure H_2 (99.9999%) at the design pressure of the component, with strict limits on inhibiting impurities (O_2 < 1 ppm, CO_2 < 1 ppm, CO < 1 ppm, and H_2O < 3 ppm).

The use of hardness as a predictor of subcritical crack propagation resistance has some limitations. In fact, it is well known that for a given hardness or strength level, there are large differences in resistances to HE depending on microstructure (Echaniz et al. 1998). Certainly, the presence of fresh martensite in hard spots should be prevented. Welds of vintage, high Mn steels are at greater risk, especially when they have a banded microstructure (Thompson and Bernstein 1977). However, subcritical crack growth was also reported for presumably innocuous microstructures. Results by Hoover et al. (1981) from Sandia Laboratories determined that subcritical cracks propagated through the HAZ in a fine-grained ferritic with spheroidized carbides region between the acicular HAZ at the fusion boundary and the base metal. More research is required on this topic.

6.2.2.5 Gaseous inhibitors of HE

Cialone and Holbrook (1988) studied fracture toughness of API 5L X42 and X70 exposed to different gas mixtures, with rising displacement tests, at a total pressure of 6.9 MPa. Fracture toughness in inert environments (CH_4 or N_2) was around 200 MPa $m^{1/2}$. The fracture toughness was halved when measured in 60% H_2 + CH_4 blends, but when the blend contained 24% of carbon monoxide (CO), the fracture toughness was restored to the original value; Figure 4 (indicated as simulated syngas in the figure). Cialone and Holbrook (1988), using constant displacement tests, also showed that CO inhibits subcritical cracking by HE in austenitized and water quenched X42 steel. This heat treatment was performed to simulate hard spots, occasionally found in existing pipelines. The high levels of CO quoted before might be present in town gas or syngas blends, a gaseous fuel obtained from coal or oil by-products. Those blends were used as fuel before natural gas displaced them in most parts of the world, but their use persists in some places like Hawaii (Melaina et al. 2013). Considering the inhibiting effect of CO, syngas is much less aggressive than a natural gas blend with a similar H_2 content.

Another key inhibitor is oxygen. When it is present in at least 50 ppm in the H_2 + N_2 mixture, it partially inhibits the aggressive effects of hydrogen (Briotett and Ez-Zaki 2018) (Figure 4). Oxygen has many of the desired attributes for an inhibitor; it is effective at low concentrations, nontoxic, cheap and produced concurrently with “green” hydrogen in water electrolyzers fed with renewable energy.

6.3 Hydrogen effects in fatigue

Fatigue of metals involves crack initiation and propagation driven by cyclic stresses. SN curves are frequently used for characterizing the fatigue behavior of metals, where the amplitude of cyclic stress (S) is plotted versus the number of stress cycles (N) that a smooth specimen resists prior to fracture. N comprises both fracture initiation and propagation. On the other hand, studies of crack propagation require fractomechanic specimens with machined pre-cracks. In those tests, the rate of crack growth per cycle (da/dN) is usually plotted as a function of stress intensity factor amplitude, $\Delta K = K_{max} - K_{min}$, the difference between maximum and minimum stress intensity factors in a cycle. ΔK is the main mechanical variable controlling fatigue crack propagation. ASTM E647 (2015) standard has guidelines for those tests, where load and crack length are measured as a function of time. Considering that existing pipelines have a defect population in base metal and welds inherent to their fabrication and service, FCGR and their dependence with H_2 partial pressure and metallurgical variables is addressed in this section. FCGR is required for damage tolerance analysis and residual life calculations.

For FCGR in an inert environment (air in Figure 5), three different regions are classically distinguished for da/dN versus ΔK. One of the simplest and most used models is given by the Paris law, valid for region II,

$$da/dn = C(\Delta K)^m \tag{10}$$

where C and m are material constants. For steels with S_y < 600 MPa (87 ksi) at temperatures up to 100 °C, $C \approx 1.65 \times 10^{-8}$ and $m \approx 3$, for da/dN in mm/cycle and ΔK in MPa $m^{1/2}$ (BS 7910 2005; API 579-1/ASME FFS-1 2021). Region I occurs at lower ΔK values, and da/dN decreases asymptotically with ΔK (Figure 5). Below the threshold stress intensity factor range, ΔK_0, da/dN is lower than 10^{-7} mm/cycle (ASTM E647 2015), which is sufficiently low for engineering calculations. For steels under the same conditions listed for Equation (10), the ΔK_0 value is 2 MPa $m^{1/2}$. In region III, da/dN rapidly increases as K_{max} approaches K_{IC} (Figure 5). There are more complex models than the one presented in Equation (10) that account for R ($R = K_{min}/K_{max}$) dependencies and the asymptotic behaviors in region I and III (Schijve 2009; API 579-1/ASME FFS-1 2021).

Hydrogen, either previously dissolved in the steel microstructure or absorbed simultaneously with cyclic loading, increases FCGR of carbon and low alloy steels (Murakami and Ritchie 2012). The increased rate depends on R, ΔK, frequency, temperature, H_2 partial pressure, impurities in the gas phase, and steel microstructure and strength

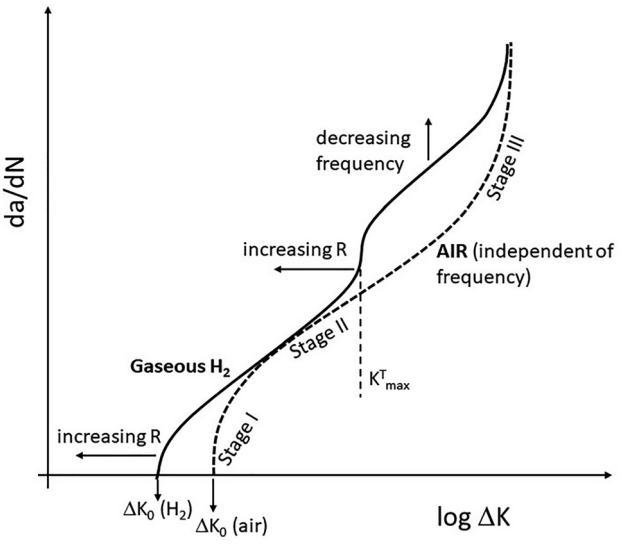

Figure 5: Schematic diagram showing the effect of gaseous, dry H_2 in da/dN of medium and low strength steels (S_y < 770 MPa). $R = K_{min}/K_{max}$, after Suresh and Ritchie (1982).

level (Nanninga et al. 2010). The effect of some of those variables on region I and II is presented in Figure 5, after Suresh and Ritchie (1982). Gaseous H_2 increases da/dN both at moderate values of ΔK and close to ΔK_0 (Figure 5).

FCGR is required to estimate residual life of flawed structures under cyclic loads. According to ASME B31.12 (2019), KD-10 article in ASME BPVC VIII.3 (2017) must be followed. Tests are performed according to ASTM E647 (2015) in gaseous H_2 under the same environment specifications as for K_{TH} measurements. Triplicate tests must be conducted for base metal, welds and HAZ, at a frequency not higher than 0.1 Hz and for the expected ΔK and R of the component.

Air fatigue yields a transgranular fracture independently of ΔK value. In presence of gaseous H_2, transgranular fracture dominates at small ΔK values (in Figure 5 those corresponding to ΔK such that $K_{max} < K^T_{max}$). When $K_{max} > K^T_{max}$, fracture advances intergranularly due to hydrogen interaction with the stressed crack tip (Suresh and Ritchie 1982). Considering that $K_{max} = \Delta K/(1 - R)$, an increase in R shifts the transition point to the left (Figure 5). For pipeline and other low-strength steels, $K^T_{max} < K_{IH}$, the fracture threshold under static or slowly rising loads. Like K_{IH} (Figure 4), K^T_{max} decreases with an increase in H_2 partial pressure (Suresh and Ritchie 1982). Finally, unlike air fatigue where da/dN is independent of frequency, da/dN in a H_2 containing environment increases with a decrease in frequency, because crack remains open for longer times as the frequency decreases, thus favoring hydrogen absorption and transport to the crack tip. Therefore, frequencies of 1 or 2 Hz (Cialone and Holbrook 1985; Suresh and Ritchie 1982) or

lower (recall that KD-10 article requires 0.1 Hz or lower) are required for conservative estimations of da/dN in H_2. The differences between H_2 and air fatigue in zone I were explained considering crack closure effects in air, which are important for low values of R (Suresh and Ritchie 1982).

FCGR increases as the H_2 partial pressure increases from 0.02 MPa to 100 MPa (San Marchi and Somerday 2012; Slifka et al. 2018). According to different authors, even at low H_2 partial pressures, da/dN increases by a factor of around 10, with respect to air measured values (Table 2). Notice that Table 2 shows results in terms of partial pressure of H_2 and not H_2 molar fraction or volume percentage, but for example 0.02 MPa would correspond to a 0.3% H_2 at a total pressure of 6.9 MPa (1000 psi), a representative value for natural gas pressure in a transmission line. The experimental matrix studied by the authors cited in Table 2 is much more extensive than the points referenced in the table. The table was prepared to show that, like the effect of H_2 on K_{IH}, the aggressive effects of H_2 on FCGR persist at very low H_2 partial pressure.

6.3.1 Effect of microstructure and steel grade on FCGR in H_2

Among the usually found microstructures and strength values in pipeline steels, there are not clear correlations between those variables and $(da/dN)H_2$ (Nanninga et al. 2010), as the results presented below show.

In a pioneering study, A516 steel was thermally treated to produce different microstructures, including ferritic–pearlitic, bainitic–ferritic, and tempered martensitic (Wachob and Nelson 1981), with previous austenitic grain size ranging from 30 to 200 μm. Corresponding S_y values were 305, 415 and 820 MPa. Despite differences in microstructure and strength level, da/dN versus ΔK curves in 6.9 MPa H_2 were similar, except for differences in ΔK_0, which was in the range of 8–13 MPa $m^{1/2}$.

Cialone and Holbrook (1988) also compared a vintage, hot rolled X42 pipeline steel with banded ferritic–pearlitic microstructure and numerous elongated MnS inclusions versus a Nb and Mo microalloyed API 5L X70 controlled-rolled steel with a polygonal ferritic microstructure intermixed with a constituent consisting of acicular ferrite and blocky islands of martensite/retained austenite. The $(da/dN)_{H2}$ versus ΔK for the modern X70 steel in 6.9 MPa H_2 at R = 0.1 was below the curve for the vintage X42 steel (Cialone and Holbrook 1988). It is challenging to make performance comparisons due to differences in grade, microstructure and chemical composition. Slifka et al. (2018) recently studied several pipelines steels, including modern and vintage API 5L X52, X70 and X100. Despite the differences in strength and microstructure, which ranged from different amounts of ferritic-pearlitic, polygonal ferritic, acicular ferritic and bainitic microconstituents, FCGR in 5.5 MPa and 34 MPa H_2 had similar dependences with ΔK, with data exhibiting considerable superposition. Those results are promising for hydrogen transport using modern, higher strength steels, because stronger steels could tolerate higher pressures or smaller thicknesses, allowing reductions on weight and material cost without penalties on FCGR.

da/dN versus ΔK curves for fusion zone and HAZ of submerged arc welds of an API 5L X60 steel in 6.9 MPa H_2 were like the ones measured for the base metal (San Marchi and Somerday 2012). Recently, FCGR tests were conducted on API 5L X70, including base metal, girth, and longitudinal welds, and HAZ's (Chandra et al. 2021). The testing environments were 12.3 MPa methane with 0, 1, 5, and 10% H_2. It was concluded that welds and HAZ's were not more susceptible than the base metal. The hardness in welds and HAZ were below 230 HV, whereas the parent pipe had 219 HV. Similarly, a 25% H_2 in natural gas mixtures at 8.5 MPa caused an increase in FCGR up to a factor of 20, for girth welds of API 5L X60 steel (Benoit et al. 2021). Drexler et al. (2019), concluded that HAZ of X52 and X70 had a similar FCGR than respective base metal in H_2 at 34 MPa and 5.5 MPa. Most of the welds and HAZ had hardness values below 250 HV, but in some areas, like the cap pass of X70 weld, hardness values near 350 HV were reported. Finally,

Table 2: Effect of low partial pressure of H_2 in fatigue crack growth rate of various carbon and low alloy steels.

Grade	da/dN_{H2} mm/cycle	da/dN_{air} mm/cycle	p H_2 MPa	ΔK MPa $m^{1/2}$	R	References
API 5L X42	1.4×10^{-3}	1.4×10^{-4}	0.2	22	0.25	Holbrook et al. (1982)
SM490B (0.16 wt% C, S_y = 360 MPa)	7×10^{-4}	5×10^{-5}	0.7	20	0.1	Yoshikawa et al. (2014)
API 5L X70	8×10^{-4}	10^{-4}	0.1	30	0.1	Nguyen et al. (2021a)
API 5L X80	4×10^{-3}	2×10^{-4}	0.6	40	0.1	Meng et al. (2017)
API 5L X52	3×10^{-3}	$4{,}6 \times 10^{-4}$ [a]	0.6	30	0.1	Ronevich and San Marchi (2021)
API 5L X70	2×10^{-4}	2×10^{-5}	0.123	16	0.3	Chandra et al. (2021)

[a]Not reported in reference. Calculated with Paris law, Equation (10).

the HAZ of a vintage API 5L X52, with higher carbon content and ferritic–pearlitic microstructure, had higher $(da/dN)H_2$ than base metal, probably due to the presence of untempered martensite in the fusion line (Drexler et al. 2019). Residual stresses in welds can also contribute to the higher FCGR in HAZ, according to a recent study by Ronevich et al. (2018) on API 5L X100.

Alternatively to experimental measurements, ASME B31.12 (2019) allows to estimate $(da/dN)H_2$ for pipeline steels in gaseous hydrogen service up to 20 MPa and $R < 0.5$ according to:

$$\left(\frac{da}{dN}\right)_{H_2} = a1\Delta K^{b1} + \left[\left(a2\Delta K^{b2}\right)^{-1} + \left(a3\Delta K^{b3}\right)^{-1}\right]^{-1} \quad (11)$$

where $a1$, $a2$, $a3$, $b1$, $b2$, and $b3$ are empirical constants (Table 3). Equation (11), used with values in Table 3, gives the upper bound of the data at 20 MPa, the maximum hydrogen gas pressure allowed by the ASME B31.12 code. This equation was developed in a testing program where the base metal of different heats of API 5L X52 (including one modern and one vintage version) and X70 pipeline steels were analyzed in 5.5 and 34 MPa H_2 and $R = 0.5$ (Amaro et al. 2018; Slifka et al. 2018). Welds and HAZ were not included in this program. Parameters for this equation are indicated in ASME B31.12 (2019), for the upper bound fit of da/dN_{H2} versus ΔK measurements obtained in the program. All experimental points in Table 2 lay between the air (Equation (10)) and ASME B31.12 master curve.

The Institution of Gas Engineers and Managers (IGEM) has published more conservative FCGR laws, IGEM (2021). They include an R dependence and are valid for a maximum operating pressure not exceeding 137.9 bar (13.79 MPa). Notice that there is an FCGR law applicable to $R \geq 0.5$, thus solving a limitation of ASME B31.12 curve. FCGR in H_2 laws published by IGEM are multistage Paris crack growth laws (Equation (10)), with coefficients C and m that must be selected considering both ΔK and R, see Table 4.

Table 3: Coefficients for FCGR law (Equation (11)) for steels in H_2 service, valid for $R < 0.5$ and design pressure not to exceed 20 MPa (3000 psi), ASME B31.12 (2019).

Material constant	Value
a1	4.08×10^{-9}
b1	3.21
a2	4.09×10^{-11}
b2	6.48
a3	4.88×10^{-8}
b3	3.61

ΔK in MPa $m^{1/2}$, da/dN in mm/cycle.

6.3.2 The effect of gaseous inhibitors and impurities on H_2 assisted FCGR

O_2, CO, C_2H_4 (ethylene), SO_2 (sulfur dioxide), and methyl mercaptan (or methanethiol, odorant commonly added to natural gas) inhibit FCGR in H_2, probably by adsorption of S, O, or C that blocks hydrogen absorption (Holbrook et al. 2012). The inhibition efficiency is principally controlled by the inhibitor nature, load frequency and R, according to a predictive model by Sommerday et al. (2013). Oxygen is a promising inhibitor, considering the low required amount (on the order of 100 ppm by volume), its efficiency and its low cost (Cerniauskas et al. 2020). Pipeline quality natural gas can have an oxygen content up to 1% or 10,000 ppm (Kidnay and Parrish 2006), which is well above the required amount for FCGR inhibition. However, if O_2 is to be adopted as an inhibitor, minimum quantities must be guaranteed. Finally, the inhibiting effect of CO on FCGR explains why town gas or syngas, which also contains H_2 and methane, is not as aggressive as a natural gas + H_2 blend.

Some natural gas impurities, like CO_2 or H_2S, could have an accelerating effect of FCGR (Barthelemy 2011; Shang et al. 2020). From an engineering perspective, it is of interest to assess the long-term benefits (or threats) of impurities in natural gas mixtures (Laureys et al. 2022), a topic that deserves further investigation.

7 Codes and recommended practices for natural gas versus hydrogen pipelines

Natural gas pipelines are commonly designed, constructed, tested, and inspected according to ASME B31.8 (2010). Requirements for hydrogen pipelines are stricter than for natural gas pipelines, and they are detailed in ASME B31.12 (2019), first introduced in 2009. Industrial gases producers from Europe and North America published a set of recommended practices and service experience on H_2 pipelines (EIGA 2014), which are useful when used with a pipeline design code.

The EIGA (European industrial gases association) document applies to H_2 concentrations above 10%, at a temperature between −40 °C and 175 °C and total pressure of 1–21 MPa. If CO > 200 ppm, the gas is outside the scope of the document, because CO inhibits the aggressive effects of H_2. This document includes requirements for steels to be used for the construction of pipelines for hydrogen transport. For example, hardness of base metal, welds and HAZ are limited to 22 HRC (Rockwell C) or 250 HB (Brinell), which

Table 4: Coefficients for multistage Paris FCGR law for steels in H_2 service, with design pressure not to exceed 13.79 MPa (2000 psi), IGEM (2021).

R	Stage A		Stage B		Stage C		Stage D		ΔK for Stage A/Stage B transition point	ΔK for Stage B/Stage C transition point	ΔK for Stage C/Stage D transition point
	C	m	C	m	C	m	C	m			
<0.5	7.59×10^{-14}	8.16			2.78×10^{-12}	7.82	1.68×10^{-7}	3.37	6.42	6.42	11.8
≥0.5	9.38×10^{-10}	5.10	2.70×10^{-8}	2.88	9.02×10^{-12}	7.82	5.46×10^{-7}	3.37	4.55	6.42	11.8

ΔK in MPa.m$^{1/2}$, *da/dN* in mm/cycle.

corresponds to UTS of 800 MPa. CE is limited to 0.43 for C–Mn steels and 0.35 for microalloyed steels. The limits on CE help to assure that UTS of weld and HAZ remain below 800 MPa. The document recommends API PSL2 versions for hydrogen pipelines, in their microalloyed versions (EIGA 2014). They indicate that there are few reported problems for hydrogen pipelines constructed with X52 and lower API 5L grades and ASTM A106 Grade B steel. The good service experience is related both to the low strength of steels used and to the low hoop stress, typically below 30%–50% of SMYS (EIGA 2014; Rawls and Adams 2012). ASME B31.12 was introduced in 2009 to allow hydrogen pipeline operation at higher hoop stress levels, with the intention that additional requirements reduce the over-conservatism level (Rawls and Adams 2012).

ASME B31.12 (2019) has three parts, part GR has general requirements, part IP applies to piping and part PL to pipelines. Piping is located within an industrial plant, like a petroleum refinery or a chemical plant, and is not further discussed in this paper. Seamless and welded API 5L grades up to X80 are among the suitable materials for pipelines listed in part GR. Grades with SMYS greater or equal to 65 ksi (450 MPa) have a maximum allowable operating pressure of 1500 psi. It is interesting to note that Ni content in carbon and low alloy steels is limited to 0.50 wt%, which parallels the 1 wt% Ni restriction for steels for sour service in ISO 15156. This restriction has motivated research (Kappes et al. 2014), and the effect of Ni in low alloy steels is not completely understood at present. Finally, like EIGA recommendations, ASME B31.12 also recommends the use of microalloyed steels, with a fine polygonal and acicular ferritic grain uniformly distributed through the thickness.

The GR part in ASME B31.12 lists several requirements for welds for hydrogen service stricter than the ones applicable to natural gas pipelines constructed according to ASME B31.8. For example, the welding procedure must include a minimum preheating temperature of 80 °C irrespective of the CE or thickness. ASME B31.8 requires preheating when carbon content is more than 0.32% or the carbon equivalent is higher than 0.65%. ASME B31.12 requires PWHT when thickness is above 20 mm, versus 32 mm in ASME B31.8. In ASME B31.12, welding procedures include a maximum allowable hardness of 235 HV for base metal, weld and HAZ. This limit is lower than the ASME B31.8 or ISO 15156-2 limit for sour service, 22 HRC or 250 HV.

Part PL contains pipeline design rules applicable when H_2 > 10% (in volume), p (total gas pressure) < 21 MPa (3000 psi), temperature is between −62 °C and 232 °C and water content is below <20 ppm. The thickness (t) of pipeline is calculated according to Barlow's equation, with four safety factors (F, E, T and H_f), all of them ≤1

$$P = \frac{2SMYSt}{D} FE_W T_f H_f \tag{12}$$

where D is external diameter, F is the design factor (it accounts for proximity of pipeline to roads, highways, rails, streets, and buildings), E_W is the longitudinal joint factor (referred to as E in the code, not to be confused with Young modulus), T_f is the temperature derating factor (referred to as T in the code, not to be confused with temperature) and H_f is the material performance factor in gaseous H_2.

ASME B31.8 has a similar expression, but without the H_f factor. This factor accounts for the effect of gaseous H_2 on mechanical properties of carbon and low alloy steels. E_W and T_f have similar values both in ASME B31.12 and ASME B31.8. For seamless, electric resistance welded, electric flash welded or double submerged arc welded pipes at temperatures up to 121 °C (250 F) the codes set both factors to 1.

When the hoop stress, σ_h, is greater than 40% SMYS, ASME B31.12 requires the use of API 5L PSL 2 pipeline and proposes two options for fracture propagation control, option A (Prescriptive Design Method), and option B (Performance-Based Design Method). H_f is used in option A and it decreases as the SMYS and the design pressure increase. H_f is set to 1 for SMYS ≤ 52 ksi (360 MPa) and P ≤ 2000 psig (13.8 MPa). For higher grades or operating pressure, H_f < 1. Option B sets H_f = 1 in all cases but requires fracture toughness measurements in gaseous H_2. Method A assigns lower values to the design factor F, which considers the location of the pipeline. Therefore, the maximum possible operating stress according to method A is limited to 50% SMYS (Table 5). Method B uses the same F values specified for natural gas pipelines, ASME B31.8, thus allowing operating stresses up to 72% SMYS.

Table 5: Pipeline safety factors and material requirements according to prescriptive (A) and performance (B) based options in ASME B31.12 (2019), required when σ_h > 40% SMYS.

	Option A	Option B
Design factor, F	Smaller than in ASME B31.8, for example 0.50 (H_2) versus 0.72 (natural gas) for location class 1, division 2	0.72 (location class 1, division 2), same as ASME B31.8
Factor H_f	≤1, dependent on steel grade and pressure	=1
Brittle fracture control at the lower of 0 °C and the service temperature	Shear aspect in Charpy specimen not less than 80% for full-thickness Charpy specimens, or 85% for reduced-size Charpy specimens	
Ductile fracture arrest capacity at the lower of 0 °C and the service temperature	Minimum Charpy energy in standard dependent on hoop stress due to design pressure, pipe radius and wall thickness	
Product specification level (PSL)	PSL2 versions required	
K_{TH}	Not specified	≥50 ksi.$\sqrt{}$in (55 MPa $\sqrt{}$m)
Inclusion shape control practices	Not specified	Required
Phosphorous content	Not explicitly specified, but according to API 5L PSL 2, $P \leq 0.025\%$	$P \leq 0.015\%$
Maximum UTS (base metal and welds)	≤100 ksi	≤110 ksi
SMYS	≤70 ksi	≤80 ksi

Minimum shear fracture area and absorbed energy in Charpy tests are specified by method A at 0 °C or the lowest expected service temperature, so that the pipeline has a ductile behavior and sufficient toughness to arrest a ductile fracture. The welding procedure must be qualified so that HAZ and base metal comply with minimum specified values of Charpy energy. Finally, the UTS of the base metal and HAZ are limited to 100 ksi and SMYS ≤ 70 ksi.

For method B, besides the Charpy test requirements indicated in the last paragraph, the base metal, weld and HAZ must be tested in gaseous H_2 at or above the design pressure and at room temperature. K_{TH}[1] and fatigue crack growth rate must be measured according to ASTM E1681 (2020) and ASTM E647 (2015) (Table 1), respectively. The pipeline must have enough fracture toughness to tolerate an elliptic flaw of 0.25 t depth and 1.5 t length, where t is pipe thickness, or a critical crack size developed by applicable fatigue loading, following rules in Article KD-10 (ASME BPVC VIII.3 2017). K_{TH} must be not less than 50 ksiin$^{1/2}$ (55 MPa m$^{1/2}$). Table 5 indicates some additional requirements of method B, comparing them with those of method A.

It is interesting to compare specifications in Table 5 with those for PSL 2 steels in API 5L 46th ed (2018). Grades X70 PSL 2 and lower have a maximum UTS ≤ 110 ksi. Hence, option B implicitly limits the SMYS to 70 ksi. Option A requires maximum UTS ≤ 100 ksi, which in API 5L is achieved by X46 and lower grades. Finally, the phosphorus requirement in method B is 0.015 wt%, stricter than the 0.025% limit in API 5L.

7.1 Steel pipeline service conversions

Appendix H in EIGA (2014) document and ASME B31.12 (2019) have detailed procedures for service conversion of pipelines originally constructed for other services, like natural gas. The complexity and costs of tasks to be performed for service conversion increase with the number of unknowns on technical information and history of the pipeline. For example, if mill certificates are missing, the material description shall be determined by chemical and physical analysis at a sampling rate of one per 1.6 km (1 mi) of pipeline (ASME B31.12 2019; EIGA 2014).

Fracture control and arrest must be qualified according to prescriptive (method A) or performance-based (method B) approaches, otherwise the MAOP must be set so that σ_h ≤ 40% SMYS (ASME B31.12 2019). Notice that qualifying a pipeline according to either method requires destructive Charpy tests on each heat of the base metal, and Charpy tests on weld and HAZ to qualify the welding procedures. On top of that, method B requires K_{TH} measurements on base metal, weld, and HAZ. Mechanical properties (hardness, S_y and UTS) of base metal and welds must be examined at a rate of 1 sample per 1.6 km (1 mi). This requirement is placed by ASME B31.12 (2019) standard regardless of the availability of mill certificates. The procedure seems extremely complex and laborious, and for pipelines made with vintage steels, it is worth recalling that impact testing requirements on pipelines were introduced just in 2000 (Kiefner and Trench 2001). Hence,

1 K_{TH} is measured at constant load or displacement. Notice that this parameter is referred to as K_{IH} in ASME B31.12 and KD-10 article in ASME BPVC. K_{TH} and K_{IH}, as defined in this work, are measured following different standards (Table 1), and for pipeline steels $K_{IH} < K_{TH}$.

qualifying an existing pipeline built before 2000 for hydrogen service according to those standards imply a paramount amount of testing or a considerable derating, so that $\sigma_h \leq 40\%$ SMYS.

8 Field experience

8.1 Conversion of pipelines for H_2 transport

Two pipelines, originally constructed as crude oil pipelines, were converted to hydrogen in Texas (USA). However, the details found are insufficient to calculate basic parameters like hoop stress (Air Liquide 2005).

An 11 km segment of a natural gas pipeline in Netherlands, originally built in 1996, was recently converted to transport a mixture of hydrogen with up to 30% methane (Huising and Krom 2020). The pipeline conforms to L415MB (X60 M, where M is for Thermomechanical rolled), and was manufactured according to similar requirements to those for PSL 2 pipelines in API 5L 2018. The design pressure was 66.2 bar (6.62 MPa) with natural gas, which resulted in a hoop stress of 55 to 46% of SMYS (there were two different thicknesses along the pipe length). For H_2 service, pressure was reduced to 41.7 bar (4.17 MPa), resulting in hoop stresses equal to 35 or 29% SMYS. Service conversion was performed following Dutch pipeline regulations. Analyzing the problem from ASME B31.12 perspective, as hoop stress <40% S_y, fracture control and arrest requirements can be omitted. This is an example of derating after service conversion. The effect of H_2 on FCGR was disregarded because ΔK was less than 3.3 MPa $m^{1/2}$, even considering a conservative flaw. FCGR in H_2 is essentially the same as FCGR in air at those ΔK values (Slifka et al. 2018). The low ΔK is explained by small variations in pipeline pressure during service.

8.2 Hydrogen blending in natural gas pipelines

The Agency for the Cooperation of Energy Regulation (ACER) conducted a survey among national regulatory authorities (NRA) of 23 European countries, aimed at identifying the technical ability of the gas transportation systems to accept H_2 blends, pure H_2 and biomethane (ACER 2020). The countries with highest allowable H_2 blending percentages are Germany (10%), France (6%), Spain (5%) and Austria (4%). The German concentration threshold is lowered to 2% if compressed natural gas filling stations are connected to the pipeline. The limit for Spain corresponds to non-conventional sources, like gas from biomass. There are reports of hydrogen blending in Italian (SNAM 2020) and German pipelines (OGE 2020).

Construction and design of natural gas pipelines in Germany, the country with the highest allowable blending percentages, are ruled by codes DVGW G 463 (A) 2016; EN 1594 (2000) (when design pressure is greater than 16 bar). According to DVGW G463 (2016), the gas in the pipeline must fulfill the requirements of the 2nd family of gases in DVGW G260. Gas can have up to 10% of H_2, it might be synthetic, or natural, and its chemical and physical properties (Wobbe index, heating value and relative density) must meet the standard (DVGW G 260 2021) requirements. Notice that this 10% limit is based on H_2 effects on gas performance in boilers, heaters, stoves, or similar, and not on H_2 effects on pipeline steel mechanical properties. Pipelines are designed according to EN 1594 (2000), where an expression like Equation (12) is used to calculate the pipeline thickness. Safety factors in DVGW G463 (2016) are more conservative than in ASME B31.8 (2010). The maximum admissible hoop stress is 62.5% SMYS (vs. 72% in ASME B31.8 2010). Steels currently used for transmission pipelines (ISO 3183 2019) are equivalent to PSL 2 pipelines listed in API 5L.

Another country with specific regulations on hydrogen pipelines, blending and repurposing is Great Britain (IGEM 2021). The regulation closely follows ASME B31.12 (2019) requirements, but a major difference is that it considers the possibility of qualifying the material for hydrogen service with mechanical tests conducted at the actual H_2 partial pressure of the pipeline (ASME B31.12 and KD-10 article in ASME BPVC VIII.3 2017 only consider tests in pure H_2 at the design pressure). IGEM document also includes requirements for repurposing a natural gas line to hydrogen or blends. Design stress determination follows a similar philosophy than ASME B31.12, with a prescriptive and performance-based option, and similar limits on UTS (690 MPa) and hardness (250 HV) of base metal, welds, and HAZ. The standard is ambiguous about blending at small partial pressures, indicating that “below 10% mol there is no evidence to confirm that blends containing up to 10% mol hydrogen do not cause material degradation, but it is considered that the risk is low”.

There are several on-going blending projects for distribution networks. It is recalled that those operate at much lower pressure than transmission pipelines. The criterion for fixing blending amounts is related to performance of appliances like boilers, gas cookers and heaters (AGN 2021; Isaac 2019).

9 Discussion

According to the evidence reviewed in this paper (Briottet and Ez-Zaki 2018; Chandra et al. 2021; Meng et al. 2017; Nguyen et al. 2021a; Ronevich and San Marchi 2021), FCGR increases, and K_{IH} decreases with H_2 partial pressure without an apparent lower threshold for H_2. Additionally, zones with hardness greater than 98 HRB (equivalent to 228 HV, or UTS of 750 MPa) or susceptible microstructure might be present in existing pipelines, with the consequent risk of subcritical cracking if H_2 is to be injected. Subcritical cracking must be prevented in loaded structures because its outcome is catastrophic failure. Hardness might be used as a screening tool to infer the presence of susceptible microstructures in linepipes, incompatible with gaseous H_2. The oil and gas industry has followed this approach for selecting materials resistant to sulfide stress cracking, a form of hydrogen embrittlement, placing a limit of 22 HRC (248 HV, or UTS of 790 MPa), among other materials requirements (ISO 15156-2). It is cautioned that an HAZ with a susceptible microstructure can present subcritical crack growth even at hardness values close to the 98 HRB screening threshold, as reported by Hoover et al. (1981). According to Hoover et al. findings, susceptible microstructures are not necessarily limited to fresh martensite.

H_2 blending in transmission natural gas pipelines requires special precautions irrespective of the desired H_2 content in the mix. Besides the risk of subcritical crack growth, how pipeline integrity is affected by the decrease in fracture toughness and the increase in FCGR by H_2 should be understood before blending or repurposing an existing pipeline. Such understanding requires a detailed knowledge of material, stress state, environmental variables, and flaw characteristics in the existing component (Figure 6). Besides internal pressure and its fluctuations, the pipeline geometry is required to determine primary stresses acting on the pipe. Residual stress can contribute to fracture in existing welded pipes (Anderson and Brown 2016), depending on pipe thermomechanical history. Thermal stresses, earth stresses rising from soil movement and installation stresses like those in field bends are required for a complete description of stress state (Fessler and Sen 2014). Current technologies for defects and crack detection in existing pipelines include in-line inspection (ILI), which is based on non-destructive detectors mounted on inspection pigs (Kania et al. 2014) and hydrotesting (destructive), commonly performed at a pressure not less than 1.25 the maximum operating pressure (ASME B31.8 2010). All the information summarized in Figure 6, added to guidelines in engineering codes, allow calculating the

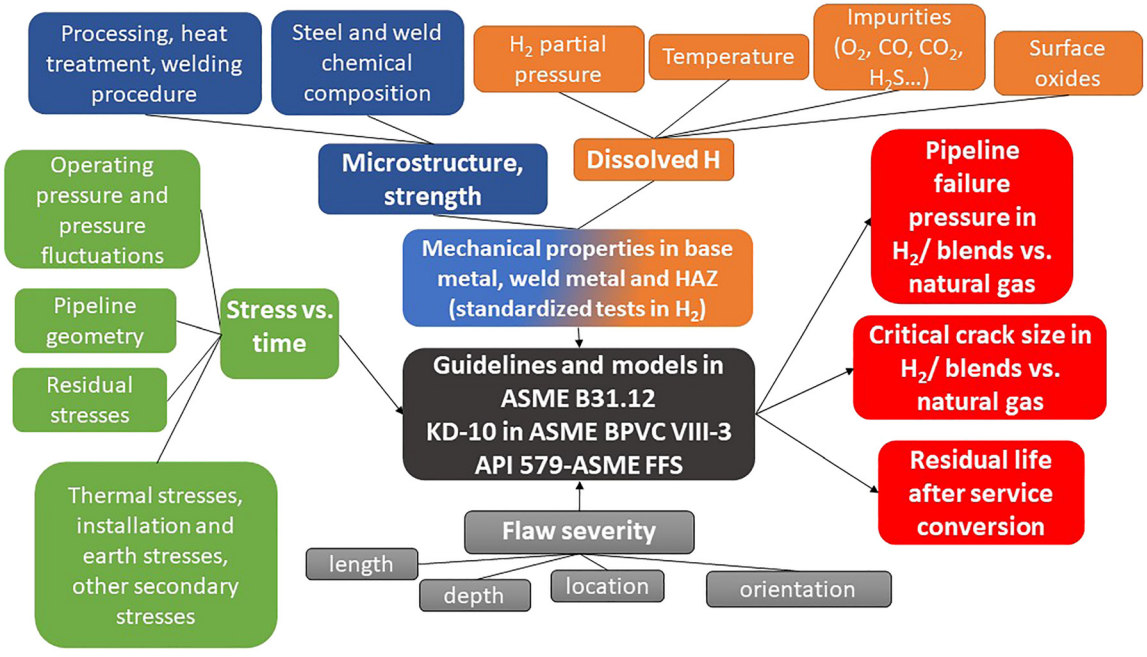

Figure 6: Influence diagram showing dependencies of main parameters required for estimating component performance in gaseous hydrogen or blends.

failure pressure, the decrease in critical crack size and the remaining life after blending. The rest of the discussion provides some additional guidelines for applying this methodology.

9.1 Where is the risk of hardness >98 HRB highest in existing pipelines?

Hydrogen embrittlement is controlled by material strength and microstructure. Hardness is often used for an indirect determination of strength. However, hardness-strength correlations, like the ones used in this work (based on ASTM A370-22 2022), are microstructure dependent and hence, the interrelationships are approximate. On top of that, a UTS determination tests a much larger zone of material than a hardness measurement. Therefore, a material with a given UTS can have zones with hardness above and below the value predicted from hardness-strength correlations. Inhomogeneities in chemical composition and in thermal cycles promote different microstructures through the specimen thickness, with associated disparities in hardness. This section explores where hardness and microstructures highly susceptible to hydrogen embrittlement might be present in existing pipelines.

9.1.1 Base metal

Elements like Mn and P segregate leading to non-uniformities in local chemical composition and banded microstructures (Thompson and Bernstein 1977). Vintage steels have higher concentrations of those elements than modern microalloyed steels. During cooling from high temperature (for example after hot rolling, field forming or welding) these chemical heterogeneities promote differences in microstructure through the thickness of the component. The UTS, obtained from a tensile test, could be within specification of API 5L (less than 760 MPa or 110 ksi for grades API 5L X70 and lower) but hardness values in segregated and banded pearlite zones could be in excess of the value expected from UTS measurement. Notice that a hardness of 98 HRB corresponds roughly to a UTS of 750 MPa. In other words, the UTS value gives little information on the distribution of microstructures and local hardness across the thickness, and hence, on the material response to hydrogen embrittlement.

Modern microalloyed steels have much lower C and Mn contents. The required strength is obtained by thermo-mechanically controlled processing, that allows getting a microstructure with precipitation hardening and small grain size, while minimizing the central segregation. A uniform distribution of fine grained polygonal and acicular ferrite is the target microstructure for H_2 service (ASME B31.12 2019). It is anticipated that with such careful control of microstructure an acceptable resistance to embrittlement in gaseous hydrogen can be achieved even if the hardness is above 98 HRB. Such expected performance must be evaluated by fracture toughness tests in gaseous hydrogen.

Another example of zones with excessive hardness are the so-called “hard spots”, more common in vintage steels due to the higher hardenability impaired by their C, Mn, and P contents. Clark et al. (2005) presents a summary of hard spot incidents in vintage pipelines. They occurred, for example, when an uncontrolled water jet caused a fast cooling of the plate after hot rolling (Clark et al. 2005). HE can occur in hard spots in service under natural gas if there is sufficient hydrogen absorption from the cathodic protection system. After an eventual shift to hydrogen or blends transport, the source of hydrogen could be the transported gas, and subcritical cracking could occur in hard spots.

According to the current API 5L specification, a zone with hardness above 35 HRC or 345 HV (UTS = 1080 MPa) is unacceptable if it is larger than 50 mm in any direction. As the 98 HRB threshold is much lower than the 35 HRC threshold a spot with high risk of subcritical cracking could be present in a pipe that is acceptable according to current API 5L specification.

9.1.2 Weld heat affected zones and arc-strikes

For a given welding procedure, the risk of having hard zones and untempered martensite increases with the CE of carbon and low alloyed steels. The hardenability increases with the CE and promotes the transformation to martensite during cooling. Again, vintage pipelines are at a higher risk than modern pipelines, except if a qualified welding procedure that controls cooling rate and ensures an acceptable maximum hardness value had been used. Hard spots in welds with 48 HRC and untempered martensite were detected in pipes with a base microstructure of ferrite and pearlite, in a vintage API 5L X52 pipeline (James and Hudgins 2016).

During in-service welding of pipelines, gas flowing in the inside effectively removes heat from the weld. In this case, the cooling rate will be high, increasing the risk of fresh martensite and hard spots in the HAZ. Codes for natural gas pipelines, like ASME B31.8 (2010), allow in-service welding of pipelines, required for repair operations or “hot tapping” (Bruce and Etheridge 2012). ASME B31.8 code refers to API 1104 (1999), where a 350 HV limit is placed for in-service welds. The aim of this limit is to prevent cold cracking, a

hydrogen embrittlement mechanism due to the hydrogen absorbed by the liquid metal pool during the welding process. This threshold is equivalent to UTS = 1100 MPa or 35.5 HRC, and it is excessively high and incompatible for gaseous H_2 service.

Inadvertent arc strikes cause arc burns. They can produce zones of excessive hardness, due to the extremely fast cooling rate experienced by the small touch point zone cooled by the surrounding base metal (API 1104 1999). ASME B31.12 (2019) calls them "metallurgical notches", suggesting that they can act as hydrogen assisted crack initiation sites, and they must be removed according to guidelines presented therein.

9.1.3 Cold and hot worked zones

Accidental pipeline contact with a backhoe bucket or similar equipment can cause dents and gouges. They constitute examples of zones with increased hardness due to cold work. Gouges involve metal removal and a locally reduced wall thickness. Dents are inward or outward deviations from the expected shell geometry. Both can affect the fitness for service of the pipeline (API 579-1/ASME FFS-1 2021). On top of the geometrical effects, hardness on gouges as high as 350 HV (Schöneich 2015) were measured for a 180 HV base metal (API 5L X52). Cracks due to hydrogen stress cracking were reported in the hardened layer (Schöneich 2015), the source of hydrogen was cathodic protection. This hardness level is also incompatible with H_2 service.

Special precautions are required if cold or hot bending processes are performed in the field. Both processes alter microstructure and can increase steel hardness. ASME B31.12 (2019) requires PWHT after those processes, to restore microstructure and hardness to acceptable levels. However, PWHT might not have been done in an existing natural gas pipeline, and it could potentially have a zone with hardness levels above 98 HRB.

9.1.4 Future perspectives

The low energy density of hydrogen requires transport at high pressure. The use of higher-strength steels could reduce the cost of pipelines, by reducing the required thickness for a given pipeline diameter and gas pressure (Briotett et al. 2012). With adequate control of microstructure, higher-strength steels with acceptable resistance to hydrogen embrittlement could be developed and qualified for H_2 service, even when the base metal hardness is in excess of 98 HRB. This was the strategy that made possible the use of steels with SMYS above 110 ksi (760 MPa) for sour service (Perez 2013). In this regard, the hydrogen concentrations attained during sour corrosion are higher than the ones expected under gaseous H_2 service, so it is worth taking the successful path followed by industry to develop steels resistant to harsher conditions.

9.2 What is the effect of decreased fracture toughness in H_2 in failure pressure?

The fracture toughness of pipeline steels measured under rising displacement in H_2 containing environments is reduced on the order of 50% of air measured values (Laureys et al. 2022; Pluvinage et al. 2019). This result has been confirmed for several grades of pipeline steels (Figure 4). It is anticipated that this decrease in fracture toughness would reduce the failure pressure (P_{fail}) of a flawed pipeline. P_{fail} can be estimated with the failure assessment diagram (FAD) in API 579-1/ASME FFS-1 (2021). According to KD-10 article in ASME BPVC section VIII-3 (2017), this methodology is used for determining the critical crack size. Alternatively, if the flaw size, pipeline geometry, fracture toughness and steel grade are known, P_{fail} can be calculated (Figure 6).

According to FAD curve (Figure 7), there are three possible mechanisms of failure for a structural component with flaws: brittle failure, elastoplastic failure, and plastic collapse. Assessments points inside the curve are safe, failure occurs outside the curve. The assessment point ordinate (K_r, toughness ratio) and abscissa (L_r, load ratio) are calculated according to:

$$L_r = \frac{\sigma_{ref}}{S_y} \quad K_r = \frac{K}{K_{IC}} \tag{13}$$

where σ_{ref} is the reference stress, related to stress in the uncracked ligament (Anderson 2005) and K is the applied stress intensity factor. Useful solutions for K and σ_{ref} applicable to pipelines are compiled in API 579-1/ASME FFS-1 (2021). S_y is insensitive to hydrogen, according to slow strain rate tests (San Marchi and Somerday 2012). Notice that in an H_2 containing environment, K_{IC} should be replaced by K_{IH} in Equation (13) (Boukortt et al. 2018). Both L_r and K_r increase proportionally with operating pressure, because both σ_{ref} and K in Equation (13) increase proportional to pressure for a flawed pipeline. Hence, loading paths of flawed pipelines are lines that pass through the origin (Hadj Meliani et al. 2011), and the intersection of this line with the FAD curve yields P_{fail} (Figure 7). The slope of the line is controlled by material parameters (S_y, K_{IC} or K_{IH}), pipeline geometry and flaw dimensions. Each case in Figure 7 represents pressurization of a pipeline with a given geometry, grade, and flaw dimensions. According to Equation (13), if K_{IH} is 50% K_{IC}, then the slope of this line doubles after blending hydrogen in the pipeline (case 1, 2 and 3). Notice that P_{fail} is proportional to

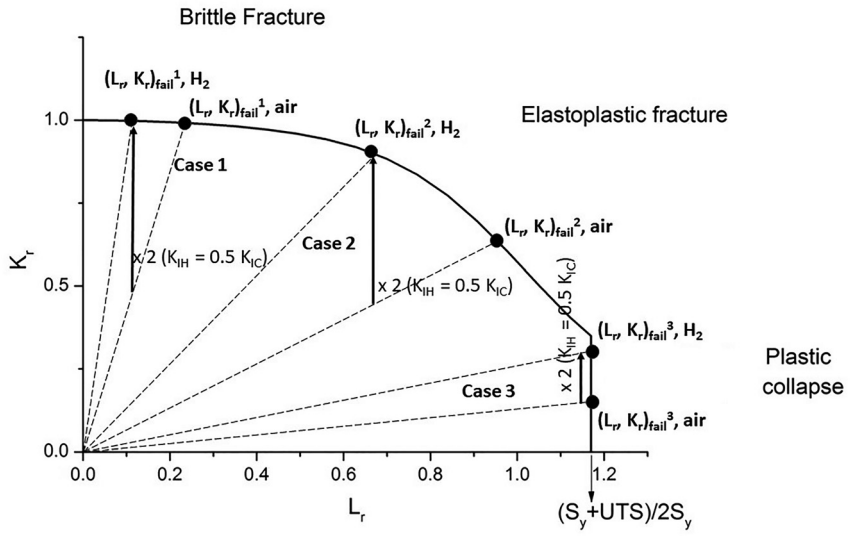

Figure 7: Failure assessment diagram (API 579-1/ASME FFS-1 2021), showing the effect of decreased fracture toughness by H_2 blending on failure pressure, P_{fail}. Each case in the figure represents a loading path for a pipeline with a given geometry, grade, and flaw size. Injecting H_2 doubles the ordinate of each point (it is assumed that $K_{IH} = 0.5\ K_{IC}$), as shown by the arrows. For each case, P_{fail} is proportional to the L_r coordinate of the point on the curve.

the corresponding L_r coordinate of the point on the FAD curve, which does not vary after injecting H_2.

The shape of the FAD curve affects the sensitivity of P_{fail} to K_{IC} (or K_{IH}, for H_2 service). This sensitivity is maximum in the brittle failure zone (case 1). There, a 50% decrease in fracture toughness by H_2 causes a 50% decrease in P_{fail}. The sensitivity decreases in the elastoplastic zone (case 2), and finally P_{fail} is independent of fracture toughness in the collapse zone (case 3). This is so because in the collapse zone, steel strength controls P_{fail} (Anderson and Brown 2016). In all cases, actual operating pressure (P) should be set to a fraction of P_{fail}, considering all applicable safety factors (F, E_W and T_f in Equation (12)).

The discussion in the previous paragraph implies that, generally, a flawed pipeline would not tolerate a hydrogen blend without a corresponding decrease in P. Otherwise, the hydrogen blend would cause failure or a decrease in safety factors. It is worth recalling that not only the assumed defect must have a conservative size and orientation (estimated from ILI inspections, hydrotesting or other), but also that reliable values of K_{IH} should be used, considering whether the defect is in the base metal, weld metal or the HAZ (Martin et al. 2022). Case 1 could represent the situation for vintage pipelines with large defects, with a deficient microstructure. Manfredi and Otegui (2002) reported K_{IC} (in air) values for vintage X46 and X52 base material between 100 and 150 MPa $m^{1/2}$, and much lower values for the weld metal, around 40 MPa $m^{1/2}$. Hydrogen injection would decrease those values, promoting brittle failure. On the other hand, case 3 would represent the case of a modern pipeline with very small defects. The base metal of a microalloyed API 5L X52 PSL 2 pipeline has a K_{IC} of 300 MPa $m^{1/2}$ in air, and 140 MPa $m^{1/2}$ in a 3% hydrogen blend at 21 MPa (Ronevich and San Marchi 2021). Calculations show that, for a 20" diameter, 0.25" thickness pipeline with 40 mm length and 2 mm depth defects (they have 90% Probability of Detection by ILI, Kania et al. 2014) P_{fail} in the H_2 blend is the same than in natural gas, despite the ~50% decrease in fracture toughness.

Knowing K_{IH} for an existing pipeline is far from reality: for most existing pipelines, not even Charpy impact energy values are known, because they were not required at the time of construction. Standardized tests for characterizing mechanical properties of base metal and welds require large amounts of steel. If representative samples of base metal, weld and HAZ of the pipeline are not available, they must be obtained from the pipeline. The development of tests for assessing mechanical properties using miniaturized specimens, like the small punch test (SPT) (Nguyen et al. 2021b), will be of particular interest for integrity programs of blended or converted pipelines. The small samples required for the SPT could be taken from an operating pipeline without compromising its structural integrity.

9.3 How to estimate the remaining life if cyclic loads are important?

Crack growth rate laws in H_2 (like Equation (11)) allow estimation of the life of cyclically loaded flawed components. The procedure is detailed in KD-4 article in ASME BPVC,

Section VIII, Division 3 (2017). Inputs for this analysis are summarized in Figure 6, and can be classified in material, stress, environmental and flaw geometry factors.

Various expressions for the stress intensity factor are listed in API 579-1/ASME FFS-1 (2021). The maximum allowable final crack depth is obtained with the failure assessment diagram (FAD), API 579-1/ASME FFS-1 (2021), considering H_2 affected fracture toughness. The critical defect size, assumed in axial orientation, should not be smaller than 0.25 t depth and 1.5 t length (t is pipeline thickness). The output of this calculation is the number of cycles to failure, defined as the lower of:

(a) one half of the number of cycles required to reach the critical crack depth.
(b) the number of cycles required for the defect to reach 25% of thickness or 25% of the critical crack depth.

The remaining life in units of time can be estimated if the pressure cycling frequency is known. Figure 8 illustrates this methodology, for this case, fatigue life is defined by criterion a) above. Some examples of estimations of H_2 effect on residual life following this methodology are presented in the literature (Chandra et al. 2021; Dadfarnia et al. 2019; Meng et al. 2017; Nguyen et al. 2021a; Ronevich and San Marchi 2021). The results depend strongly on pressure amplitude, which controls cyclic hoop stress and ΔK.

9.4 Is the higher FCGR in H_2 a concern for pipelines?

Cyclic stress range ($\Delta\sigma$) and stress intensity range (ΔK) are the main driving forces for fatigue initiation and fatigue crack propagation. Both $\Delta\sigma$ and ΔK increase proportionally with internal pressure. Pressure in pipelines exhibit daily fluctuations on the order of ±10% of the operating pressure, and less frequent shutdowns and startups for maintenance or upset conditions, in which the pressure decreases from operating pressure to zero and then back to operating pressure (Shipilov and Le May 2006). Considering pipelines loaded by internal pressure, Rosenfeld and Kiefner (2006) concluded that fatigue is not a concern for natural gas transmission pipelines, because they do not commonly experience large variations in pressure. ΔK increases with the size of cracks or flaws; however, it is concluded that if their size is small enough to survive a hydrostatic test, significant fatigue crack growth is not expected within the pipeline service life (Rosenfeld and Kiefner 2006). FCGR could be an issue if large defects are present in pipelines. For example, for the 2 mm deep and 40 mm long crack analyzed in Section 8.2, the ΔK value is 5.8 MPa $m^{1/2}$ (considering a cyclic pressure ±10% of the corresponding operating pressure at 72% SMYS). This ΔK value is right at the onset of FCGR acceleration by H_2 (Equations (10) and (11)) and the R would be close to 1. Examination of Table 2 highlights a research need: most tests of FCGR in H_2 were conducted at $R \leq 0.5$, including the ones performed for the development of ASME B31.12 (2019) FCGR master curve. How the so-called ripple load (with R close to 1) common in pressurized transmission pipelines affects FCGR in H_2 is still an open question (Chandra et al. 2021).

Full scale deployment of renewable energy production requires sufficient energy storage capacity. In a hydrogen economy, peak shaving and valley filling could be accomplished by producing and consuming green H_2. Line packing H_2 in existing transmission lines adds to the storage capacity of the system. Line packing refers to the short-term storage

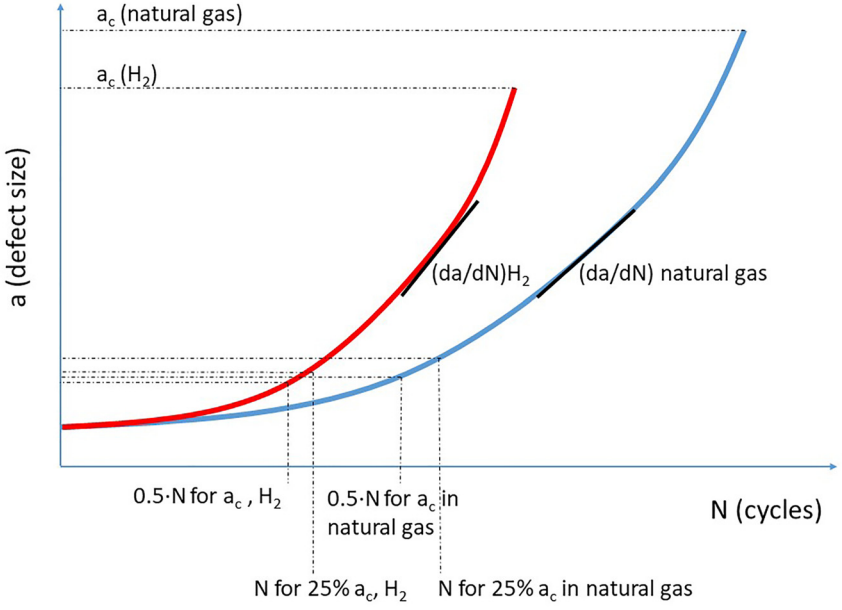

Figure 8: Schematic effect of H_2 on critical crack size (a_c), FCGR and fatigue life.

capacity of the pipeline: pipeline pressure increases and decreases during low and high periods of demand, respectively (Haeseldonckx and D'haeseleer 2007). Pipeline storage capacity scales with the difference in lower and upper pressures and the geometric volume enclosed by the pipeline. It is anticipated that this operation mode will increase the driving force for hydrogen assisted fatigue, so that the pressure amplitude will have to be limited considering the desired fatigue life.

10 Conclusions

Laboratory tests reviewed in this paper have systematically showed that gaseous hydrogen degrades ductility, fracture toughness and fatigue life. Those effects persist at low partial pressure or percentage of hydrogen in the blend. Additionally, hard zones and susceptible microstructures near welds or in the pipe base metal are susceptible to subcritical cracking in gaseous hydrogen. From a pipeline integrity perspective, the most relevant points discussed in this review are:

- The risk of subcritical cracking is high when hardness is above 98 HRB. For existing natural gas pipelines, the risk of exceeding this hardness limit is higher in welds and HAZ, particularly when equivalent carbon is high like in vintage pipelines or when welds are performed as part of field repairing. Cold-worked regions like dents and gouges might also have incompatible hardness. Segregated zones in vintage pipelines and hard spots in base metal are also at risk of subcritical cracking. Existing codes for hydrogen containing pipelines fix strict maximum values on strength and hardness of base metal and welds.
- According to a fitness for service methodology, for a flawed pipeline the decrease in failure pressure with respect to air can be evaluated if the K_{IH}/K_{IC} ratio and actual yield stress are known. However, this approach has practical limitations: it is important to recall that K_{IH} is not known for existing natural gas pipelines. Obtaining its value for base metal, weld and HAZ requires destructive sampling of the pipelines, unless welded samples representative of the welding procedure are available.
- The higher FCGR in hydrogen blends versus natural gas can decrease pipeline service life if pressure amplitudes are significant, or if flaws have such a size that hydrogen effects are important. Typically, pressurized natural gas pipelines experience stress cycles with high R values. FCGR has dependence with R, but the effect of FCGR at high values of R has received less attention than at $R < 0.5$. Future needs of using pipelines for storing hydrogen produced by renewable energies might generate stress cycles with larger amplitudes and lower R values.
- At odds with the potential effects of blending hydrogen on pipeline integrity, there are not international codes for materials selection and pipeline design applicable to H_2 contents less than 10%. An option for repurposing would be to apply ASME B31.12 to the existing natural gas pipeline. This is extremely laborious considering the number of destructive tests to be performed on the pipeline material, at a sampling rate of 1 per mile.
- Most laboratory results of hydrogen-affected properties were reported for environments with minimum concentrations of contaminants like O_2 and CO. Authors that studied the effect of those contaminants in laboratory tests reported that small amounts of them (in the ppm range) inhibit the aggressive effects of H_2, restoring properties to values measured in air. As they might be present in natural gas, this fact is promising from an engineering perspective. The role of other impurities in natural gas (CO_2, H_2S) and their interplay with inhibitors is a topic that deserves further study.

Acknowledgements: Part of this work was performed by the authors under a contract with TGN (Transportadora de Gas del Norte). They acknowledge TGN permission to publish this paper. The authors acknowledge technical discussions with Dr. C. San Marchi (Sandia National Laboratories, USA) and Narasi Sridhar. Manuscript reading and suggestions from Daniel Guerrero, Dr. Dannisa Chalfoun and Dr. Martin Rodriguez are highly appreciated.

Author contributions: All the authors have accepted responsibility for the entire content of this submitted manuscript and approved submission.

Research funding: None declared.

Conflict of interest statement: The authors declare no conflicts of interest regarding this article.

Appendix

The following figure was constructed considering the tables in ASTM A370-22 (2022), listing approximate ultimate tensile strength (UTS) as a function of hardness, measured in different scales. Such conversion is valid for nonaustenitic steels. This standard was used for listing approximate UTS and hardness in different scales in the main body of this manuscript. Notice that hardness in Brinell and Vickers scales are coincident up to 234 HB (Figure A1).

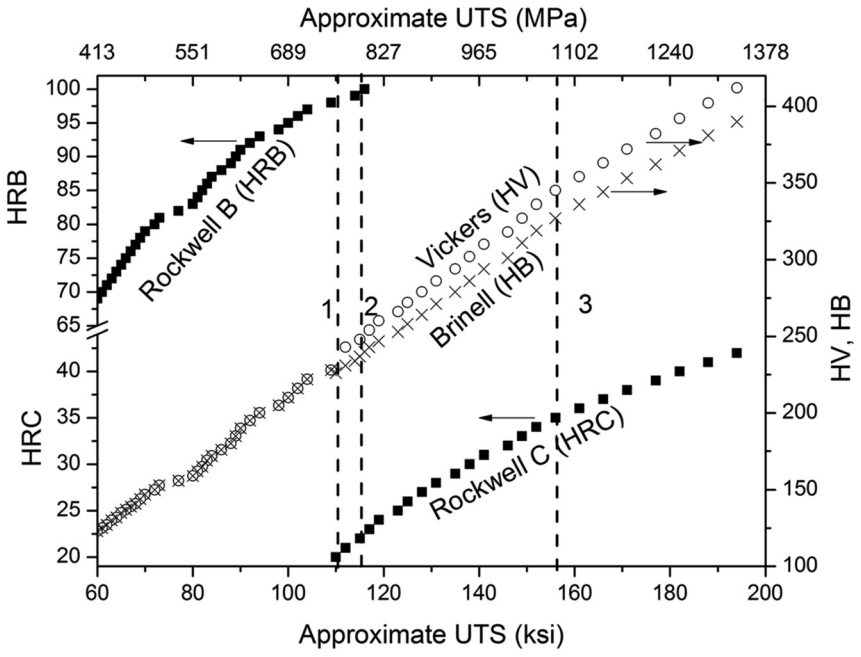

Figure A1: Approximate UTS versus hardness correlations (ASTM A370-22 (2022)). Line 1 represents maximum hardness in base metal, HAZ, and welds accepted by ASME B31.12 (2019), line 2 is the maximum hardness recommended by EIGA (2014) for service in H_2 and the limit for sour service in ISO 15156 (2015), a hardness above line 3 would qualify as "hard spot" in API 5L 2018, API 1104 1999.

References

ACER (2020). Report on NRAs survey – hydrogen, biomethane, and related network adaptations, evaluation of responses. Report, European Union Agency for the Cooperation of Energy Regulators.

AGN (2021). Hydrogen Park South Australia, Available at: https://blendedgas.agn.com.au/about-the-project (Accessed 12 December 2022).

Air Liquide (2005). Questions and issues on hydrogen pipelines, pipeline transmission of hydrogen, Available at: https://www1.eere.energy.gov/hydrogenandfuelcells/pdfs/hpwgw_questissues_campbell.pdf (Accessed 12 December 2022).

Amaro, R.L., White, R.M., Looney, C.P., Drexler, E.S., and Slifka, A.J. (2018). Development of a model for hydrogen-assisted fatigue crack growth in pipeline steel. ASME J. Pressure Vessel Technol. 140: 021403-1–021403-13.

Anderson, T.L. (2005). *Fracture mechanics: fundamentals and applications*, 4th ed. CRC Press Taylor & Francis Group, Boca Raton, FL.

Anderson, T.L. and Brown, G.W. (2016). Effect of residual forming stresses on fracture in ERW pipe, IPC2016-64553. In: *Proceedings of the international pipeline conference & exposition, IPC2016 September 26–30, 2016, Calgary, Alberta, Canada*.

API 5L (2018). *Specification 5L Line pipe*, 46th ed. American Petroleum Institute, New York City.

API 579-1/ASME FFS-1 (2021). *Fitness-for-service*. The American Petroleum Institute and The American Society of Mechanical Engineers, New York City.

API 941 (2016). Recommended practice 941, Steels for hydrogen service at elevated temperatures and pressures in petroleum refineries and petrochemical plants. 8th ed. American Petroleum Institute, New York City.

API 1104 (1999). *Welding of pipelines and related facilities*, 19th ed. American Petroleum Institute, New York City.

Asahi, H., Ueno, M., and Yonezawa, T. (1994). Prediction of sulfide stress cracking in high-strength tubulars. Corrosion 50: 537–545.

ASME B31.8 (2010). *Gas transmission and distribution piping systems. ASME Code for pressure piping B31*. American Society of Mechanical Engineers (ASME), New York City.

ASME B31.12 (2019). *Hydrogen piping and pipelines. ASME code for pressure piping B31*. American Society of Mechanical Engineers (ASME), New York City.

ASME BPVC VIII.3 (2017). *ASME boiler & pressure vessel code. Section VIII: rules for construction of pressure vessels. Division 3: alternative rules for construction of high pressure vessels*. American Society of Mechanical Engineers (ASME), New York City.

ASTM A370-22 (2022). *Standard test methods and definitions for mechanical testing of steel products*. ASTM International, West Conshohocken, Pennsylvania.

ASTM E647-15 (2015). *Standard test method for measurement of fatigue crack growth rates*. ASTM International, West Conshohocken, Pennsylvania.

ASTM E1681-03 (2020). *Standard test method for determining threshold stress intensity factor for environment-assisted cracking of metallic materials*. ASTM International, West Conshohocken, Pennsylvania.

ASTM E1820-20b (2020). *Standard test method for measurement of fracture toughness*. ASTM International, West Conshohocken, Pennsylvania.

ASTM G142-98 (2016). *Standard test method for determination of susceptibility of metals to embrittlement in hydrogen containing environments at high pressure, high temperature, or both*. ASTM International, West Conshohocken, Pennsylvania.

Banks, T.M. and Gladman, T. (1979). Sulphide shape control. Met. Technol. 1979: 81–94.

Barthelemy, H. (2011). Effects of pressure and purity on the hydrogen embrittlement of steels. Int. J. Hydrogen Energy 36: 2750–2758.

Benoit, G., Bertheau, D., Hénaff, G., and Alvarez, L. (2021). Crack growth resistance of actual pipe weldments exposed to a high pressure mixture of hydrogen and natural gas. In: *Proceedings of the ASME 2021, pressure vessels & piping conference PVP2021, paper PVP 2021-61945, July 12–16, 2021, virtual, online*.

Boukortt, I.H., Amara, M., Hadj Meliani, M., Muthanna, B.G.N., Bouledroua, O., Suleiman, R.K., Sorour, A.A., and Pluvinage, G. (2018). Hydrogen embrittlement effect on the structural integrity of API 5L X52 steel pipeline. Int. J. Hydrogen Energy 43: 19615–19624.

Bouledroua, O., Hafsi, Z., Djukic, M.B., and Elaoud, S. (2020). The synergistic effects of hydrogen embrittlement and transient gas flow conditions on integrity assessment of a precracked steel pipeline. Int. J. Hydrogen Energy 45: 18010–18020.

Briottet, L. and Ez-Zaki, H. (2018). Influence of hydrogen and oxygen impurity content in a natural gas/hydrogen blend on the toughness of an API X70 steel. In: *Proceedings of the ASME 2018 pressure vessels and piping conference PVP2018, July 15–20, 2018*, Prague, Czech Republic.

Briottet, L., Batisse, R., de Dinechin, G., Langlois, P., and Thiers, L. (2012). Recommendations on X80 steel for the design of hydrogen gas transmission pipelines. Int. J. Hydrogen Energy 37: 9423–9430.

Bruce, W.A. and Etheridge, B.C. (2012). Further development of heat-affected zone hardness limits for in-service welding. In: *Proceedings of the 2012 9th international pipeline conference IPC2012 september 24–28, 2012*. Calgary, Alberta, Canada.

BS 7910:2005 (2005). *British standard. Guide to methods for assessing the acceptability of flaws in metallic structures*. British Standards Institution, London, UK.

Cancio, M.J., Giacomel, B., Kissner, G., Valdez and M., and Vouilloz, F. (2014). High strength low alloy steel for HPHT wells. In: *Offshore technology conference-Asia, OTC-24746-MS, offshore technology conference, 25–28, 2014*, Kuala Lumpur, Malaysia.

Cerniauskas, S., Chavez Junco, A.J., Grube, T., Robinius, M., and Stolten, D. (2020). Options of natural gas pipeline reassignment for hydrogen: cost assessment for a Germany case study. Int. J. Hydrogen Energy 45: 12095–12107.

Chandra, A., Thodla, R., Prewitt, T.J., Matthews, W., and Sosa, S. (2021). Fatigue crack growth study of X70 line pipe steel in hydrogen containing natural gas blends. In: *Proceedings of the ASME 2021 pressure vessels & piping conference PVP2021, July 12–16, 2021*, virtual, online.

Chalfoun, D.R., Kappes, M.A., Bruzzoni, P., and Iannuzzi, M. (2022). Hydrogen solubility, diffusivity, and trapping in quenched and tempered Ni-containing steels. Int. J. Hydrogen Energy 47: 3141–3156.

Chen, W., Wang, S.H., King, F., Jack, T.R., and Wilmott, M.J. (2000). Hydrogen permeation behavior of X70 pipeline steel in a near-neutral pH soil environment. In: *2000 International pipeline conference*, Vol. 2. ASME International, New York, NY, pp. 953–960.

Cialone, H.J. and Holbrook, J.H. (1985). Effects of gaseous hydrogen on fatigue crack growth in pipeline steel. Metall. Trans. A 16A: 115–122.

Cialone, H.J. and Holbrook, J.H. (1988). Sensitivity of steels to degradation in gaseous hydrogen. In: Raymond, L. (Ed.), *Hydrogen embrittlement: prevention and control. ASTM STP 962*. American Society for Testing and Materials, Philadelphia, pp. 134–152.

Clark, E.B., Leis, B.N., and Eibner, R.J. (2005). *Final report on integrity characteristics of vintage pipelines, prepared for the Interstate Natural Gas Association of America*. Battelle Memorial Institute, Columbus, OH.

Clark, W.G., Jr. and Landes, J.D. (1976). An evaluation of rising load KISCC testing. In: *Stress corrosion: new approaches*. ASTM STP 610. American Society for Testing and Materials, Philadelphia, pp. 108–127.

Coburn, T.C. (2020). Oil and gas infrastructure. A technical overview. In: Hancock, K.J. and Allison, J.E. (Eds.), *The Oxford handbook of energy politics. Oxford handbooks series*. Oxford University Press, Oxford, UK, pp. 99–124.

Dadfarnia, M., Sofronis, P., Brouwer, J., and Sosa, S. (2019). Assessment of resistance to fatigue crack growth of natural gas line pipe steels carrying gas mixed with hydrogen. Int. J. Hydrogen Energy 44: 10808–10822.

Drexler, E.S., Slifka, A.J., Amaro, R.L., Sowards, J.W., Connolly, M.J., Martin, M.L., and Lauria, D.S. (2019). Fatigue testing of pipeline welds and heat-affected zones in pressurized hydrogen gas. J. Res. Nat. Inst. Stand. Technol. 124: 1–19.

DVGW G 260 (2021). *Gasbeschaffenheit*. Deutscher Verein des Gas-und Wasserfaches, Bonn, Germany.

DVGW G 463 (A) (2016). High pressure gas lines made of steel pipes for design pressure greater than 16 bar. Deutscher Verein des Gas-und Wasserfaches, Bonn, Germany.

Echaniz, G., Morales, C. and Pérez, T. (1998). The effect of microstructure on the KISSC of low alloy carbon steels. In: *NACE Corrosion '98, 22–27 March 1998*, San Diego, USA.

EIGA (2014). *Hydrogen pipeline systems IGC Doc 121/14*. European industrial gases association, Brussels.

Fessler, R.R. and Sen, M. (2014). Characteristics, causes and management of circumferential stress-corrosion cracking. IPC2014-33059. In: *Proceedings of the international pipeline conference & exposition, IPC2014 September 29–October 3, 2014*, Calgary, Alberta, Canada.

Gadgeel, V.L. and Johnson, D.L. (1979). Gas-phase hydrogen permeation and diffusion in carbon steels as a function of carbon content from 500 to 900 K. J. Mater. Energy Syst. 1: 32–40.

Gangloff, R.P. (2003). Hydrogen assisted cracking of high strength alloys. In: Milne, I., Ritchie, R.O. and Karihaloo, B. (Eds.), *Comprehensive structural integrity*, Vol. 6. Elsevier Science, New York, NY, pp. 31–101.

Gerboni, R. (2016). Introduction to hydrogen transportation. In: Gupta, R.B., Basile, A. and Nejat Veziroglu, T. (Eds.), *Compendium of hydrogen energy. Vol. 2: Hydrogen storage, distribution and infrastructure*. Woodhead Publishing, Cambridge, UK, pp. 283–300.

Groeneveld, T.P. and Elsea, A.R. (1974). Hydrogen-stress cracking in natural gas transmission pipelines. In: Bernstein, I.M. and Thompson, A.W. (Eds.), *Hydrogen in metals. Proceedings of an international conference on the effects of hydrogen on materials properties and selection and structural design, 23–27 September 1973, Champion, Pennsylvania*. American Society for Metals, pp. 727–737.

Gutierrez-Solana, F. and Elices, M. (1982). High-pressure hydrogen behavior of a pipeline steel. In: Interrante, C.G. and Pressouyre, G.M. (Eds.), *Current solutions to hydrogen problems in steels*. American Society for Metals, Metals Park, OH, pp. 181–185.

Hadj Meliani, M., Matvienko, Y.G., and Pluvinage, G. (2011). Corrosion defect assessment on pipes using limit analysis and notch fracture mechanics. Eng. Fail. Anal. 18: 271–283.

Haeseldonckx, D. and D'haeseleer, W. (2007). The use of the natural-gas pipeline infrastructure for hydrogen transport in a changing market structure. Int. J. Hydrogen Energy 32: 1381–1386.

Hara, T., Asahi, H., and Ogawa, H. (2004). Conditions of hydrogen-induced corrosion occurrence of X65 grade line pipe steels in sour environments. Corrosion 60: 1113–1121.

He, D.X., Chen, W., and Luo, J.L. (2004). Effect of cathodic potential on hydrogen content in a pipeline steel exposed to NS4 near-neutral pH soil solution. Corrosion 60: 778–786.

Holbrook, J.H., Cialone, H.J., Mayfield, M.E., and Scott, P.M. (1982). *The effect of hydrogen on low-cycle-fatigue life and subcritical crack growth in pipeline steels*, prepared for Brookhaven National Laboratory under contract with the United States Department of Energy.

Holbrook, J.H., Cialone, H.J., and Scott, P.M. (1984). Hydrogen degradation of pipeline steels. Summary report, Battelle Columbus Laboratories. Prepared for Brookhaven National Laboratory under contract with the United States Department of Energy.

Holbrook, J.H., Collings, E.W., Cialone, H.J., and Drauglis, E.J. (1986). Hydrogen degradation of pipeline steels. Final report, prepared for Brookhaven National Laboratory under contract with the United States Department of Energy.

Holbrook, J.H., Cialone, H.J., Collings, E.W., Drauglis, E.J., Scott, P.M., and Mayfield, M.E. (2012). Control of hydrogen embrittlement of metals by chemical inhibitors and coatings. In: Gangloff, R.P. and Somerday, B.P. (Eds.), *Gaseous hydrogen embrittlement of materials in energy technologies, Vol. 2: mechanisms, modelling and future developments*. Woodhead Publishing, Cambridge, UK, pp. 129–153.

Hoover, W.R., Robinson, S.L., Stoltz, R.E., and Spingarn, J.R. (1981). Hydrogen compatibility of structural materials for energy storage and transmission. Final report, prepared by Sandia National Laboratories and Livermore, California for the United States Department of Energy.

Huising, O.J.C. and Krom, A.H.M. (2020). H2 in an existing natural gas pipeline. In: *Proceedings of the 2020 13th international pipeline conference IPC2020 september 28–30, 2020, virtual, online*.

IGEM (2021). *Steel pipelines for high pressure gas transmission*. Supplement to IGEM/TD/1 Edition 6. Communication 1848, 2021.

Isaac, T. (2019). HyDeploy: the UK's first hydrogen blending deployment project. Clean Energy 3: 114–125.

ISO 3183 (2019). Petroleum and natural gas industries — Steel pipe for pipeline transportation systems. BSI Standards Institution, London, United Kingdom.

ISO 15156 (2015). *International standard. Petroleum and natural gas industries — materials for use in H2S-containing environments in oil and gas production*.

ISO 15589-1 (2015). *International standard. Petroleum, petrochemical and natural gas industries — cathodic protection of pipeline systems — Part 1: on-land pipelines*, 2nd ed.

James, B. and Hudgins, A. (2016). Failure analysis of oil and gas transmission pipelines. In: Makhlouf, A.S.H. and Aliofkhazraei, M. (Eds.), *Handbook of materials failure analysis with case studies from the oil and gas industry*. Elsevier, Amsterdam, pp. 1–38.

Kania, R., Myden, K., Weber, R., and Klein, S. (2014). Validation of EMAT-ILI technology for gas pipeline crack inspection: a case study for 20. In: *9th Pipeline Technology Conference, May 12–14th 2014*, Berlin, Germany.

Kappes, M., Frankel, G.S., Thodla, R., Mueller, M., Sridhar, N., and Carranza, R.M. (2012). Hydrogen permeation and corrosion fatigue crack growth rates of X65 pipeline steel exposed to acid brines containing thiosulfate or hydrogen sulfide. Corrosion 68: 1015–1028.

Kappes, M., Iannuzzi, M., Rebak, R.B. and Carranza, R.M. (2014). Sulfide stress cracking of nickel-containing low-alloy steels. Corrosion Rev. 32: 101–128.

Kidnay, A.J. and Parrish, W.R. (2006). *Fundamentals of natural gas processing*. CRC Press, Boca Raton, FL, USA.

Kiefner, J.F. and Trench, C.J. (2001). *Oil pipeline characteristics and risk factors: illustrations from the decade of construction*. Report for the American Petroleum Institute's Pipeline Committee.

Kiuchi, K. and McLellan, R.B. (1983). The solubility and diffusivity of hydrogen in well-annealed and deformed iron. Acta Metall. 31: 961–984.

Lam, P.S., Sindelar, R.L., and Adams, T.M. (2007). Literature survey of gaseous hydrogen effects on the mechanical properties of carbon and low alloy steels. In: *Proceedings of PVP2007 2007 ASME pressure vessels and piping division conference July 22–26, 2007*, San Antonio, Texas.

Laureys, A., Depraetere, R., Cauwels, M., Depover, T., Hertele, S., and Verbeken, K. (2022). Use of existing steel pipeline infrastructure for gaseous hydrogen storage and transport: a review of factors affecting hydrogen induced degradation. J. Nat. Gas Sci. Eng. 101: 104534.

Leis, B.N. (2015). Managing an aging pipeline infrastructure. In: Winston Revie, R. (Ed.). *Oil and gas pipelines: integrity and safety handbook*, 1st ed. John Wiley & Sons, Inc., Hoboken, New Jersey, pp. 609–634.

Loginow, A.W. and Phelps, E.H. (1975). Steels for seamless hydrogen pressure vessels. Corrosion 31: 404–412.

Ma, H.C., Zagidulin, D., Goldman, M., and Shoesmith, D.W. (2021). Influence of iron oxides and calcareous deposits on the hydrogen permeation rate in X65 steel in a simulated groundwater. Int. J. Hydrogen Energy 46: 6669–6679.

Manfredi, C. and Otegui, J.L. (2002). Failures by SCC in buried pipelines. Eng. Fail. Anal. 9: 495–509.

Martin, M.L. and Sofronis, P. (2022). Hydrogen-induced cracking and blistering in steels: a review. J. Nat. Gas Sci. Eng. 101: 104547.

Martin, M.L., Connolly, M., Buck, Z.N., Bradley, P.E., Lauria, D., and Slifka, A.J. (2022). Evaluating a natural gas pipeline steel for blended hydrogen service. J. Nat. Gas Sci. Eng. 101: 104529.

Melaina, M.W., Antonia, O., and Penev, M. (2013). *Blending hydrogen into natural gas pipeline networks: a review of key issues*, Technical Report NREL/TP-5600-51995.

Meng, B., Gu, C., Zhang, L., Zhou, C., Li, X., Zhao, Y., Zheng, J., Chen, Z., and Han, Y. (2017). Hydrogen effects on X80 pipeline steel in high-pressure natural gas/hydrogen mixtures. Int. J. Hydrogen Energy 42: 7404–7412.

Michler, T., Lindner, M., Eberle, U., and Meusinger, J. (2012). Assessing hydrogen embrittlement in automotive hydrogen tanks. In: Gangloff, R.P. and Somerday, B.P. (Eds.), *Gaseous hydrogen embrittlement of materials in energy technologies. Vol. 1: The problem, its characterization and effects on particular alloy classes*. Woodhead Publishing, Cambridge, UK, pp. 94–125.

Murakami, Y. and Ritchie, R.O. (2012). Effects of hydrogen on fatigue-crack propagation in steels. In: Gangloff, R.P. and Somerday, B.P. (Eds.), *Gaseous hydrogen embrittlement of materials in energy technologies. Vol. 1: The problem, its characterization and effects on particular alloy classes*. Woodhead Publishing, Cambridge, UK, pp. 379–418.

NACE, TM0284 (2016). *Test method evaluation of pipeline and pressure vessel steels for resistance to hydrogen-induced cracking*. NACE International, Houston, Texas.

NACE/ASTM G193 (2020). *Standard terminology and acronyms relating to corrosion*. ASTM International, West Conshohocken, Pennsylvania.

Nanninga, N., Slifka, A., Levy, Y., and White, C. (2010). A review of fatigue crack growth for pipeline steels exposed to hydrogen. J. Res. Nat. Inst. Stand. Technol. 115: 437–452.

Nguyen, T.T., Tak, N., Park, J., Nahm, S.H., and Beak, U.B. (2020a). Hydrogen embrittlement susceptibility of X70 pipeline steel weld under a low partial hydrogen environment. Int. J. Hydrogen Energy 45: 23739–23753.

Nguyen, T.T., Park, J., Sik Kim, W., Nahm, S.H., and Beak, U.B. (2020b). Effect of low partial hydrogen in a mixture with methane on the mechanical properties of X70 pipeline steel. Int. J. Hydrogen Energy 45: 2368–2381.

Nguyen, T.T., Heo, H.M., Park, J., Nahm, S.H., and Beak, U.B. (2021a). Fracture properties and fatigue life assessment of API X70 pipeline

steel under the effect of an environment containing hydrogen. J. Mech. Sci. Technol. 35: 1445–1455.

Nguyen, T.T., Park, J.S., Nahm, S.H., and Baek, U.B. (2021b). Evaluation of hydrogen related degradation of API X42 pipeline under hydrogen/natural gas mixture conditions using small punch test. Theor. Appl. Fract. Mech. 113: 102961.

Nibur, K.A. and Somerday, B.P. (2012). Fracture and fatigue test methods in hydrogen gas. In: Gangloff, R.P. and Somerday, B.P. (Eds.), *Gaseous hydrogen embrittlement of materials in energy technologies*. *Vol. 1. The problem, its characterization and effects on particular alloy classes*. Woodhead Publishing, Cambridge, UK, pp. 195–236.

Nibur, K.A., Somerday, B.P., San Marchi, C., Foulk, J.W., III, Dadfarnia, M., and Sofronis, P. (2013). The relationship between crack-tip strain and subcritical cracking thresholds for steels in high-pressure hydrogen gas. Metall. Mater. Trans. A 44A: 248–269.

OGE (2020). Press release. First green hydrogen to be fed into gas transmission system in Northern Germany. Available at: https://oge.net/en/press-releases/2020/erste-einspeisung-von-gruenem-wasserstoff-in-das-bestehende-norddeutsche-gas-fernleitungsnetz (Accessed 12 December 2022).

Oriani, R. (1970). The diffusion and trapping of hydrogen in steel. Acta Metall. 18: 147–157.

Parker, N. (2004). *Using natural gas transmission pipeline costs to estimate hydrogen pipeline costs*. Institute of Transportation Studies, UC Davis. Available at: <https://escholarship.org/uc/item/9m40m75r> (Accessed 12 December 2022).

Perez, T. (2013). Corrosion in the oil and gas industry: an increasing challenge for materials. J. Occup. Med. 65: 1033–1042.

Pluvinage, G., Capelle, J., and Hadj Meliani, M. (2019). Pipe networks transporting hydrogen pure or blended with natural gas, design and maintenance. Eng. Fail. Anal. 106: 104164.

Porter, D.A. and Easterling, K.E. (1992). *Phase transformations in metals and alloys*, 2nd ed. Chapman & Hall, London.

Rawls, G.B. and Adams, T. (2012). Hydrogen production and containment. In: Gangloff, R.P. and Somerday, B.P. (Eds.), *Gaseous hydrogen embrittlement of materials in energy technologies*. *Vol. 1: The problem, its characterization and effects on particular alloy classes*. Woodhead Publishing, Cambridge, UK, pp. 3–50.

Robertson, I.M., Sofronis, P., Nagao, A., Martin, M.L., Wang, S., Gross, D.W., and Nygren, K.E. (2015). Hydrogen embrittlement understood. 2014 Edward DeMille Campbell memorial lecture. ASM Int. Metall. Mater. Trans. 46A: 2323–2341.

Robinson, S.L. and Stoltz, R.E. (1981). Toughness losses and fracture behavior of low strength carbon-manganese steels in hydrogen. In: Bernstein, I.M. and Thompson, A.W. (Eds.), *Hydrogen effects in metals*. The Metallurgical Society of AIME, Warrendale, PA, pp. 987–995.

Ronevich, J.A. and San Marchi, C.W. (2021). Materials compatibility concerns for hydrogen blended into natural gas. In: *Proceedings of the ASME 2021 pressure vessels & piping conference PVP 2021, July 13–15, 2021*, virtual, online.

Ronevich, J.A., D'Elia, C.R., and Hill, M.R. (2018). Fatigue crack growth rates of X100 steel welds in high pressure hydrogen gas considering residual stress effects. Eng. Fract. Mech. 194: 42–51.

Ronevich, J.A., Song, E.J., Somerday, B.P., and San Marchi, C.W. (2021). Hydrogen-assisted fracture resistance of pipeline welds in gaseous hydrogen. Int. J. Hydrogen Energy 46: 7601–7614.

Rosenfeld, M.J. and Kiefner, J.F. (2006). *Basics of metal fatigue in natural gas pipeline systems — a primer for gas pipeline operators*. A technical report, prepared for the Materials Technical Committee of Pipeline Research Council International.

San Marchi, C. and Somerday, B.P. (2012). Technical reference for hydrogen compatibility of materials. Sandia Report, SAND2012-7321, prepared by Sandia National Laboratories.

Schefer, R.W., Houf, W.G., San Marchi, C., Chernicoff, W.P., and Englom, L. (2006). Characterization of leaks from compressed hydrogen dispensing systems and related components. Int. J. Hydrogen Energy 31: 1247–1260.

Schijve, J. (2009). *Fatigue of structures and materials*, 2nd ed. Springer Science, Berlin, Germany.

Schöneich, H.G. (2015). Considerations on the risk of hydrogen embrittlement of pipeline steel due to cathodic overprotection. In: *Proceedings of the pipeline technology conference, 8–10 Jun 2015*, Estrel, Berlin, Germany.

Shang, J., Chen, W., Zheng, J., Hua, Z., Zhang, L., Zhou, C., and Gu, C. (2020). Enhanced hydrogen embrittlement of low-carbon steel to natural gas/hydrogen mixtures. Scripta Mater. 189: 67–71.

Shipilov, S.A. and Le May, I. (2006). Structural integrity of aging buried pipelines having cathodic protection. Eng. Fail. Anal. 13: 1159–1176.

Slifka, A.J., Drexler, E.S., Amaro, R.L., Hayden, L.E., Stalheim, D.G., Lauria, D.S., and Hrabe, N.W. (2018). Fatigue measurement of pipeline steels for the application of transporting gaseous hydrogen. ASME J. Pressure Vessel Technol 140: 011407-1–011407-12.

SNAM (2020). SNAM: hydrogen blend doubled to 10% in Contursi trial, Available at: https://www.snam.it/en/Media/news_events/2020/Snam_hydrogen_blend_doubled_in_Contursi_trial.html (Accessed 12 December 2022).

Somerday, B.P., Sofronis, P., Nibur, K.A., San Marchi, C.W., and Kirchheim, R. (2013). Elucidating the variables affecting accelerated fatigue crack growth of steels in hydrogen gas with low oxygen concentrations. Acta Mater. 61: 6153–6170.

Stetson, N.T., McWhorter, S., and Ahn, C.C. (2015). Introduction to hydrogen storage. In: Gupta, R.B., Basile, A., and Nejat Veziroglu, T. (Eds.), *Compendium of hydrogen energy. Vol. 2: Hydrogen storage, distribution and infrastructure*. Woodhead Publishing, Cambridge, UK, pp. 3–26.

Suresh, S. and Ritchie, R.O. (1982). Mechanistic dissimilarities between environmentally influenced fatigue-crack propagation at near-threshold and higher growth rates in lower strength steels. Met. Sci. 16: 529–538.

Tazedakis, A.S., Voudouris, N., Dourdounis, E., Mannucci, G., Di Vito, L.F., and Fonzo, A. (2021). Qualification of high-strength linepipes for hydrogen transportation based on ASME B31.12 code. Pipeline Technol. J. Issue 1: 42–50.

Thompson, A.W. and Bernstein, I.M. (1977). Selection of structural materials for hydrogen pipelines and storage vessels. Int. J. Hydrogen Energy 2: 163–173.

Turnbull, A. (2012). Hydrogen diffusion and trapping in metals. In: Gangloff, R.P. and Somerday, B.P. (Eds.), *Gaseous hydrogen embrittlement of materials in energy technologies, Vol. 2: mechanisms, modelling and future developments*. Woodhead Publishing, Cambridge, UK, pp. 89–128.

Turnbull, A. (2015). Perspectives on hydrogen uptake, diffusion and trapping. Int. J. Hydrogen Energy 40: 16961–16970.

Villalobos, J.C., Del-Pozo, A., Campillo, B., Mayen, J., and Serna, S. (2018). Review: microalloyed steels through history until 2018: review of chemical composition, processing and hydrogen service. Metals 8: 1–49.

Wachob, H.F. and Nelson, H.G. (1981). Influence of microstructure on the fatigue crack growth of A516 in hydrogen. In: Bernstein, I.M. and Thompson, A.W. (Eds.), *Hydrogen effects in metals*. The Metallurgical Society of AIME, Warrendale, PA, pp. 703–711.

Xu, K. (2012). Hydrogen embrittlement of carbon steels and their welds. In: Gangloff, R.P. and Somerday, B.P. (Eds.), *Gaseous hydrogen*

embrittlement of materials in energy technologies. Vol. 1: The problem, its characterization and effects on particular alloy classes. Cambridge, UK: Woodhead Publishing, pp. 526–561.

Yoshikawa, M., Matsuo, T., Tsutsumi, N., Matsunaga, H., and Matsuoka, S. (2014). Effects of hydrogen gas pressure and test frequency on fatigue crack growth properties of low carbon steel in 0.1-90 MPa hydrogen gas. JSME Trans. 80: 1–16.

EN 1594 (2000). *Gas supply systems pipelines for maximum operating pressure over 16 Bar. Functional requirements*. British Standard Institution (English version), London, United Kingdom.

Bionotes

Mariano A. Kappes
Instituto Sabato, UNSAM/CNEA, Av. General Paz 1499, San Martín, Buenos Aires B1650KNA, Argentina
National Commission of Atomic Energy of Argentina, Av. General Paz 1499, San Martín, Buenos Aires B1650KNA, Argentina
National Scientific and Technical Research Council, Godoy Cruz, 2290, Buenos Aires C1425FQB, Argentina
marianokappes@gmail.com
https://orcid.org/0000-0002-5708-5565

Mariano A. Kappes obtained his Bachelor's degree in Materials Science and Engineering at the Instituto Sabato in Argentina in 2006. He obtained his PhD in 2011 working in the Fontana Corrosion Center at the Ohio State University. Since 2014, he is a research scientist at the National Agency of Atomic Energy in Argentina and a Professor at Instituto Sabato. His current research topics are environmentally assisted cracking and localized corrosion in structural materials used for the nuclear and oil and gas industries.

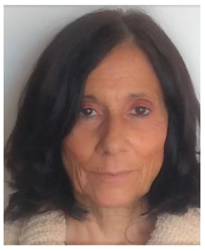

Teresa Perez
Instituto Sabato, UNSAM/CNEA, Av. General Paz 1499, San Martín, Buenos Aires B1650KNA, Argentina
TEP Consultora SRL, Buenos Aires, Argentina

Teresa Perez has more than 30 years' experience in Corrosion Science and Engineering from academic and industrial fields, mainly in O&G materials. She was Principal Scientist at Tenaris Research Center and, currently, is a consultant. She was a professor at the Engineering School (UBA) and, currently, is at Institute Sabato. Prof. Perez received the NACE Technical Achievement and Fellow Awards, the Platinum Konex Award in Science and Technology. She is Full Academician of the National Academies of Exact, Physical and Natural Sciences and Engineering.